Comprehensive *in situ* constraints on LPO fabric of fast-spreading oceanic lithosphere from seismic anisotropy

Joshua B. Russell[1], Hannah F. Mark[2,3], James B. Gaherty[1], Daniel Lizarralde[2], Pei-Ying (Patty) Lin[4], John A. Collins[2], Greg Hirth[5], Rob L. Evans[2]

[1]*Lamont-Doherty Earth Observatory of Columbia University, Palisades, NY, USA*
[2]*Woods Hole Oceanographic Institution, Woods Hole, MA, USA*
[3]*MIT/WHOI Joint Program in Oceanography/Applied Ocean Science and Engineering, MA, USA*
[4]*Department of Earth Sciences, National Taiwan Normal University, Taipei, Taiwan*
[5]*Geological Sciences Department, Brown University, Providence, Rhode Island, USA*

Lamont-Doherty Earth Observatory
COLUMBIA UNIVERSITY | EARTH INSTITUTE

OBSIP OCEAN BOTTOM SEISMOGRAPH INSTRUMENT POOL

NSF

Motivation

Geodynamic models simulate LPO fabric formation and evolution at mid-ocean ridge

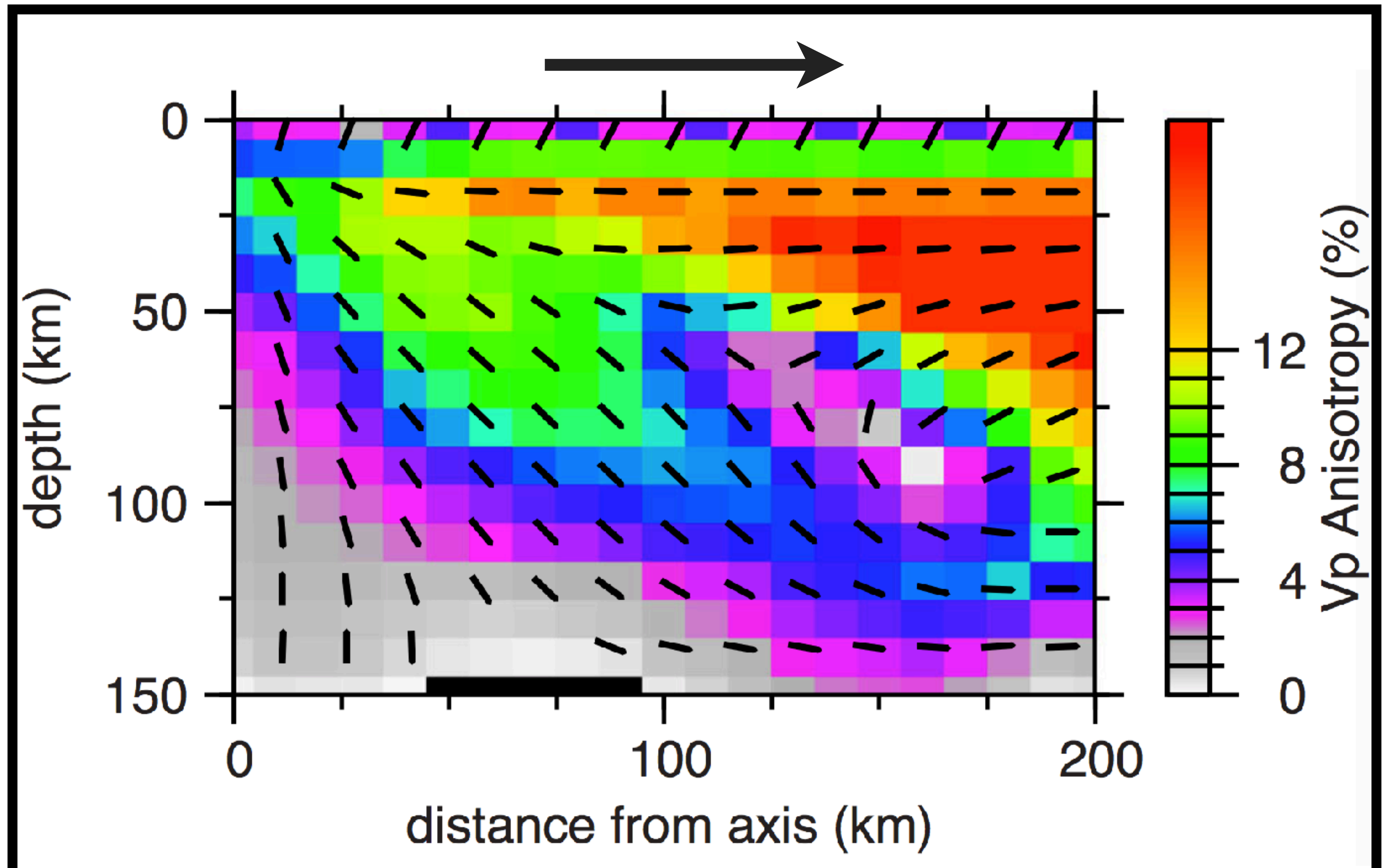

Blackman et al., 2017 GJI

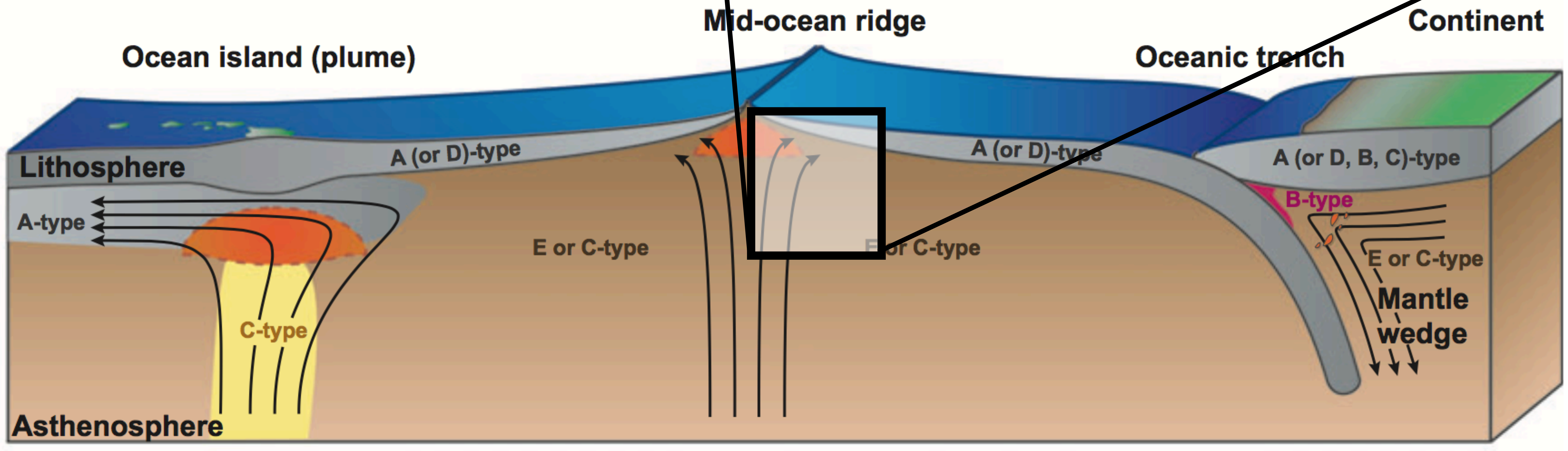

Karato et al., 2008 Annu. Rev.

Motivation

Geodynamic models simulate LPO fabric formation and evolution at mid-ocean ridge

Observations:

- Hand-sample peridotite fabrics
  - 10^{-3}–10^{2} m length scale

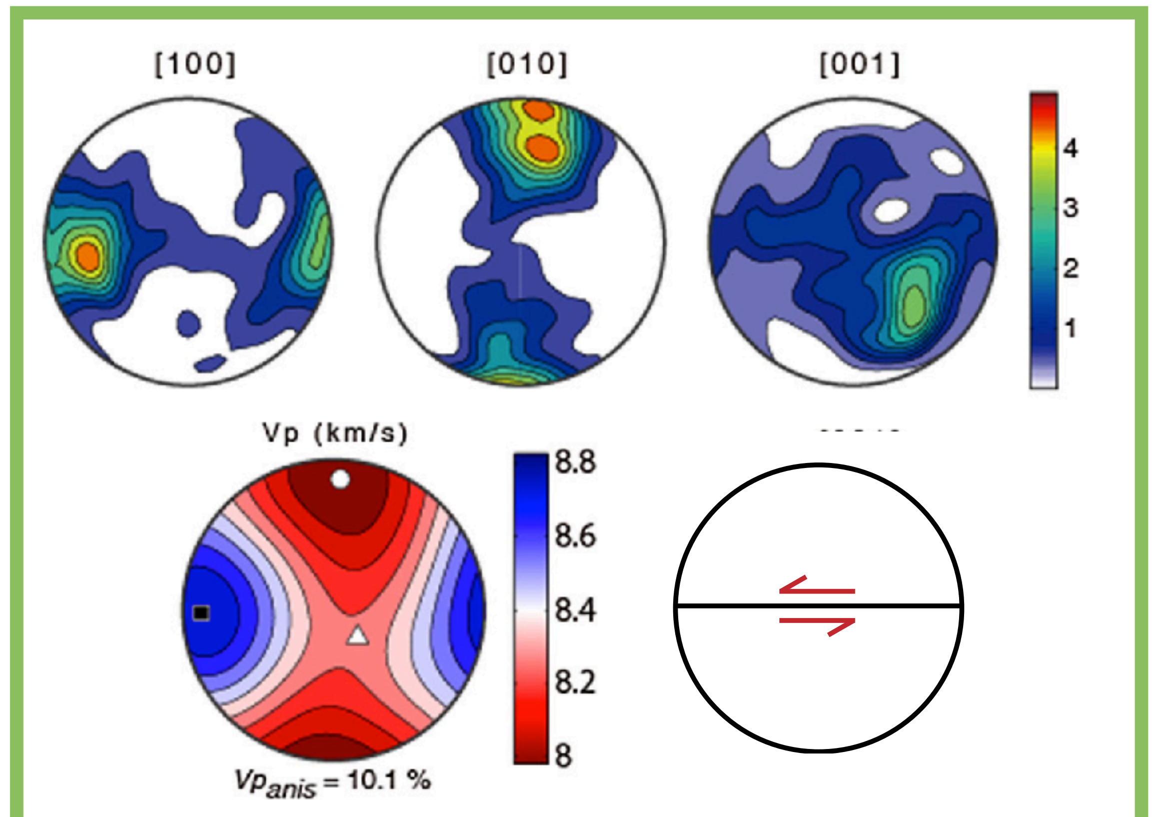

Michibayashi et al., 2016 EPSL

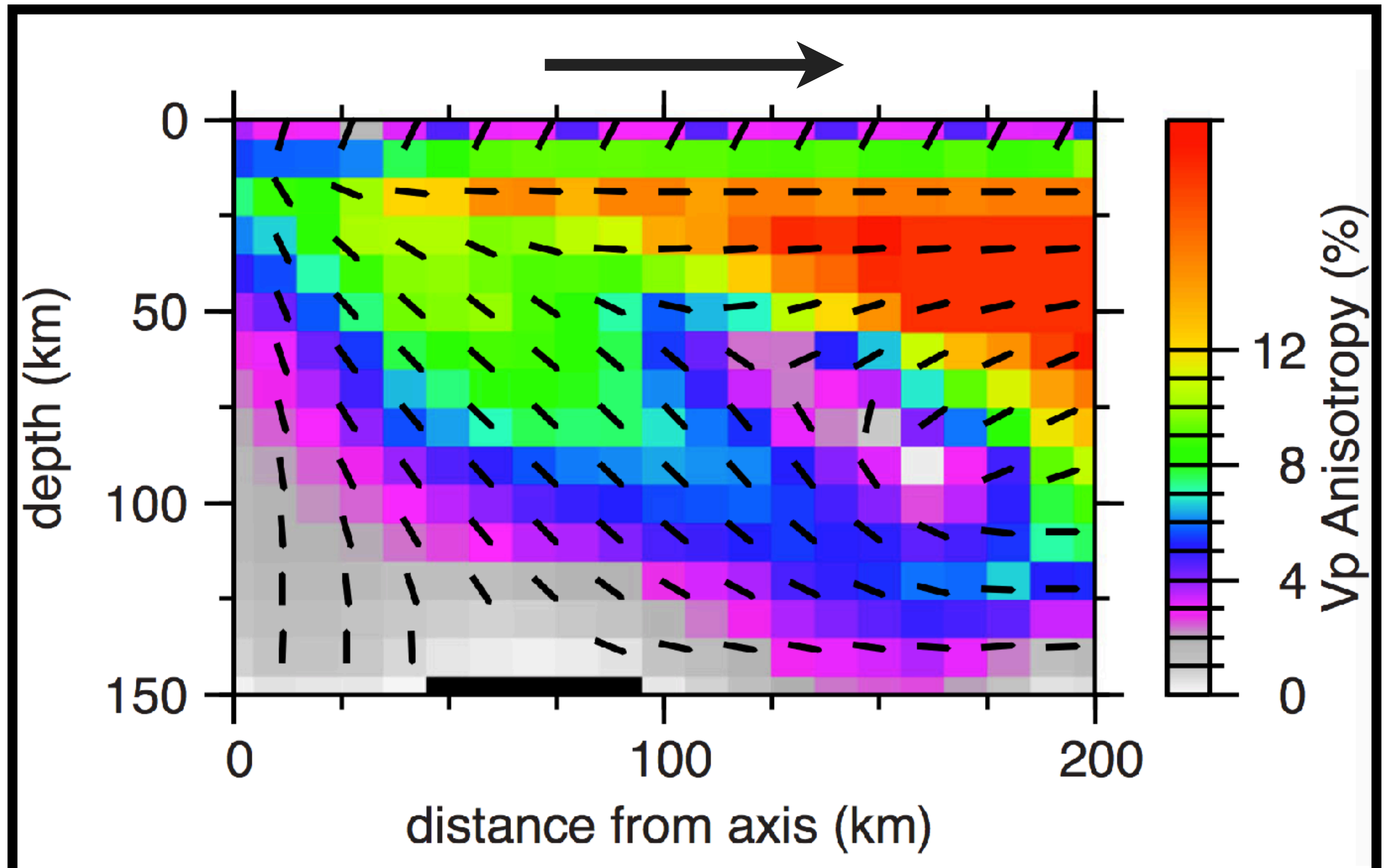

Blackman et al., 2017 GJI

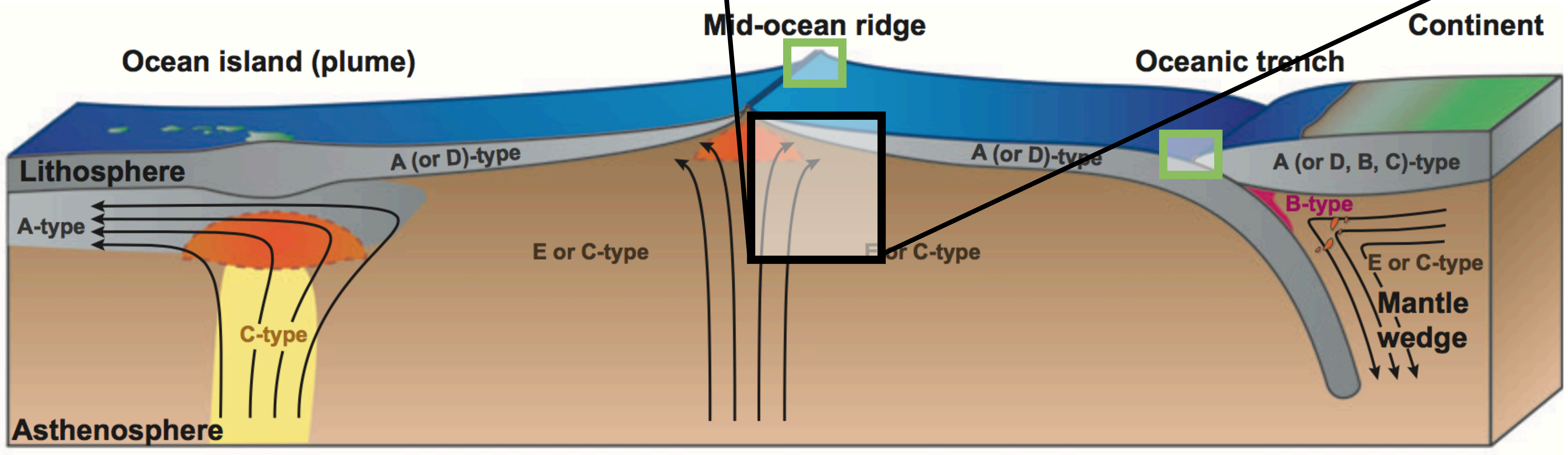

Karato et al., 2008 Annu. Rev.

Motivation

Geodynamic models simulate LPO fabric formation and evolution at mid-ocean ridge

Observations:

- Hand-sample peridotite fabrics
    - 10^{-3}–10^{2} m length scale
- Seismic anisotropy observations
    - 10^{3}–10^{7} m length scale

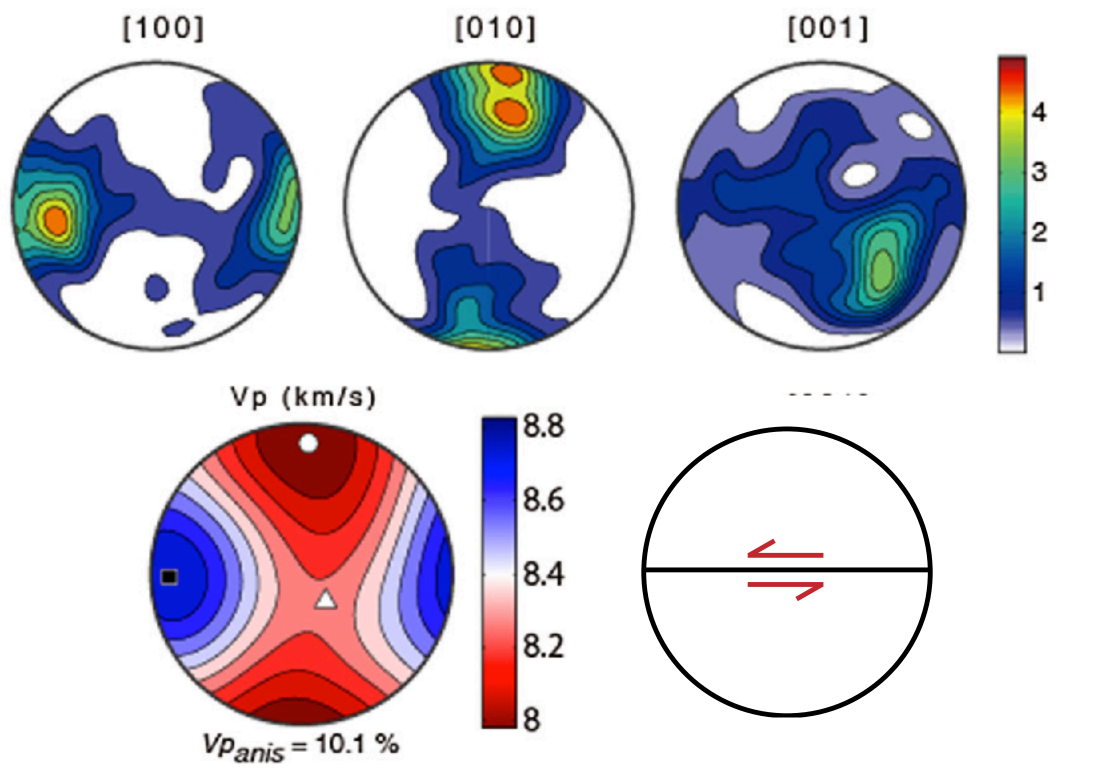

Michibayashi et al., 2016 EPSL

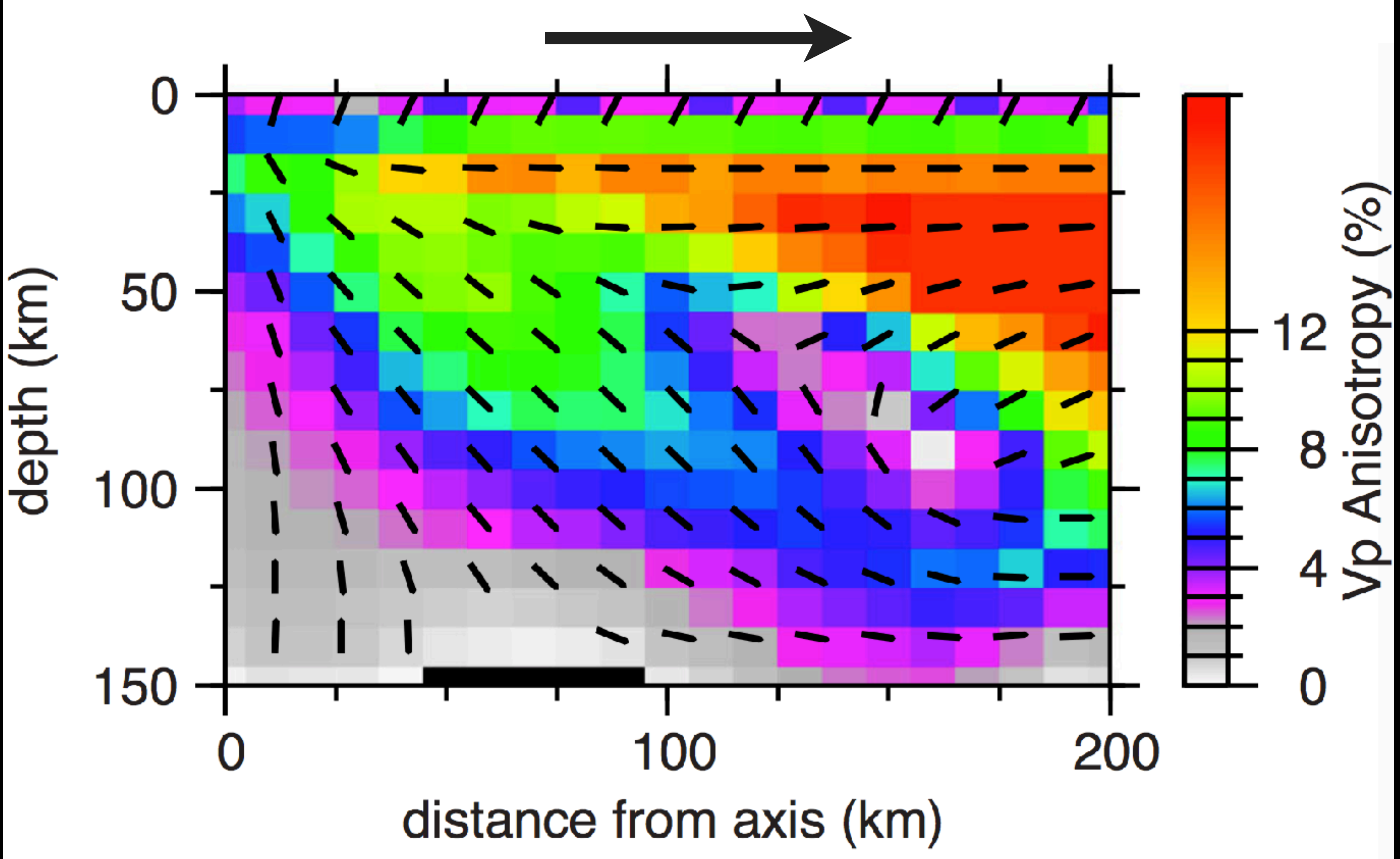

Blackman et al., 2017 GJI

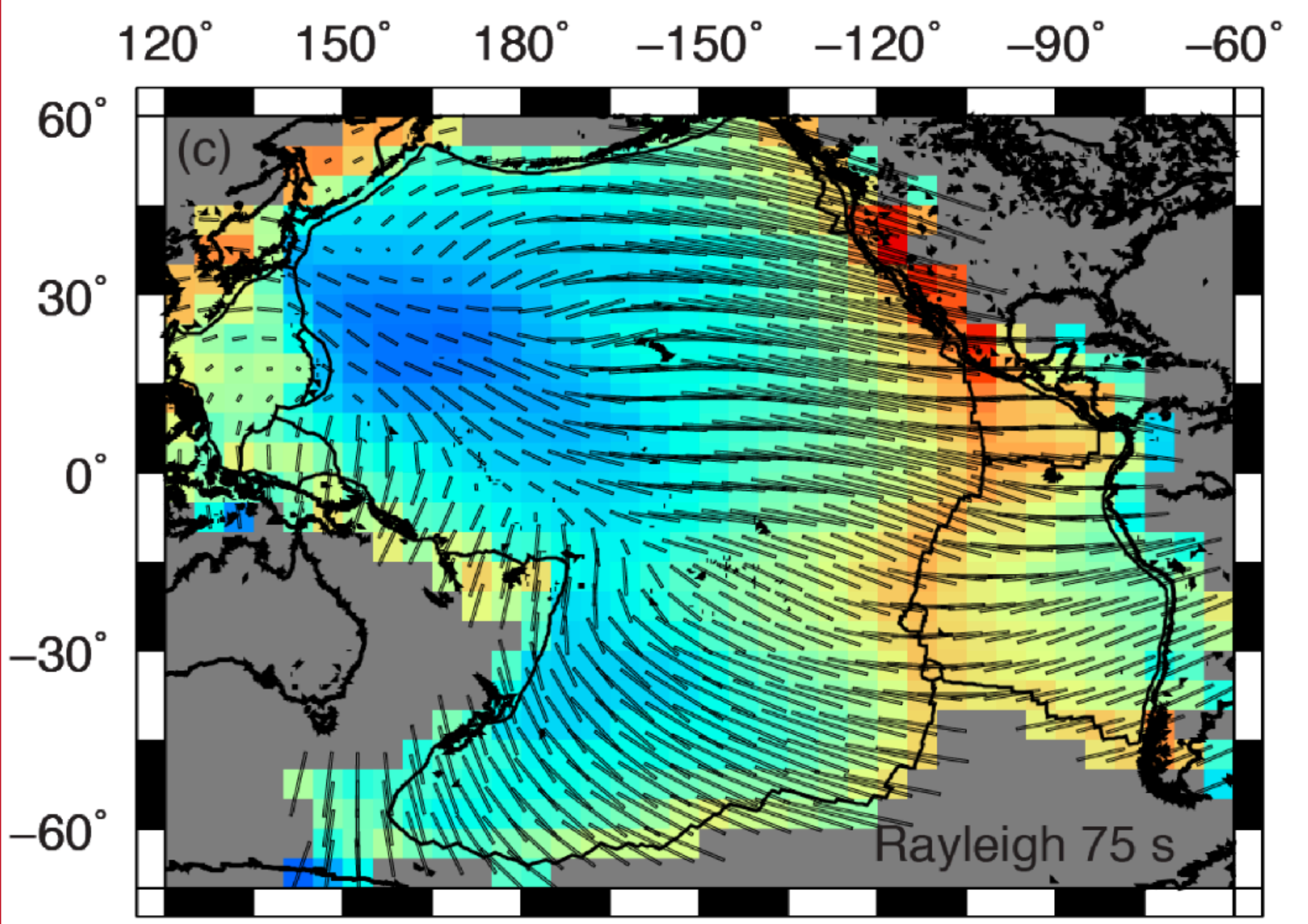

Eddy et al., 2018 GJI

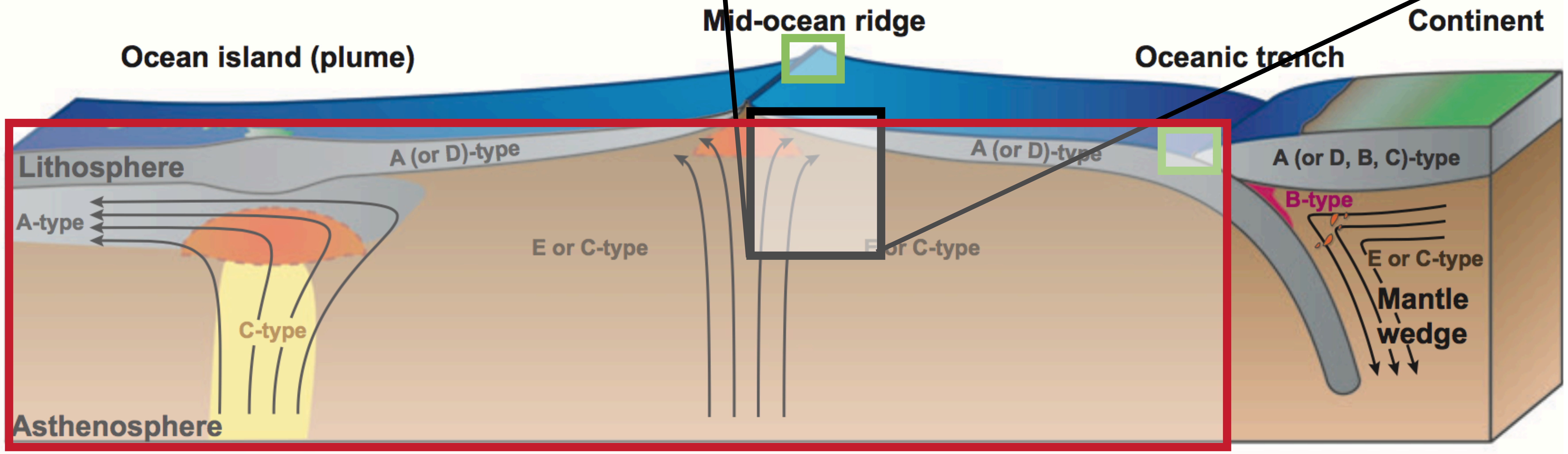

Karato et al., 2008 Annu. Rev.

Motivation

Geodynamic models simulate LPO fabric formation and evolution at mid-ocean ridge

Observations:

- Hand-sample peridotite fabrics
  - 10^{-3}–10^{2} m length scale
- Seismic anisotropy observations
  - 10^{3}–10^{7} m length scale

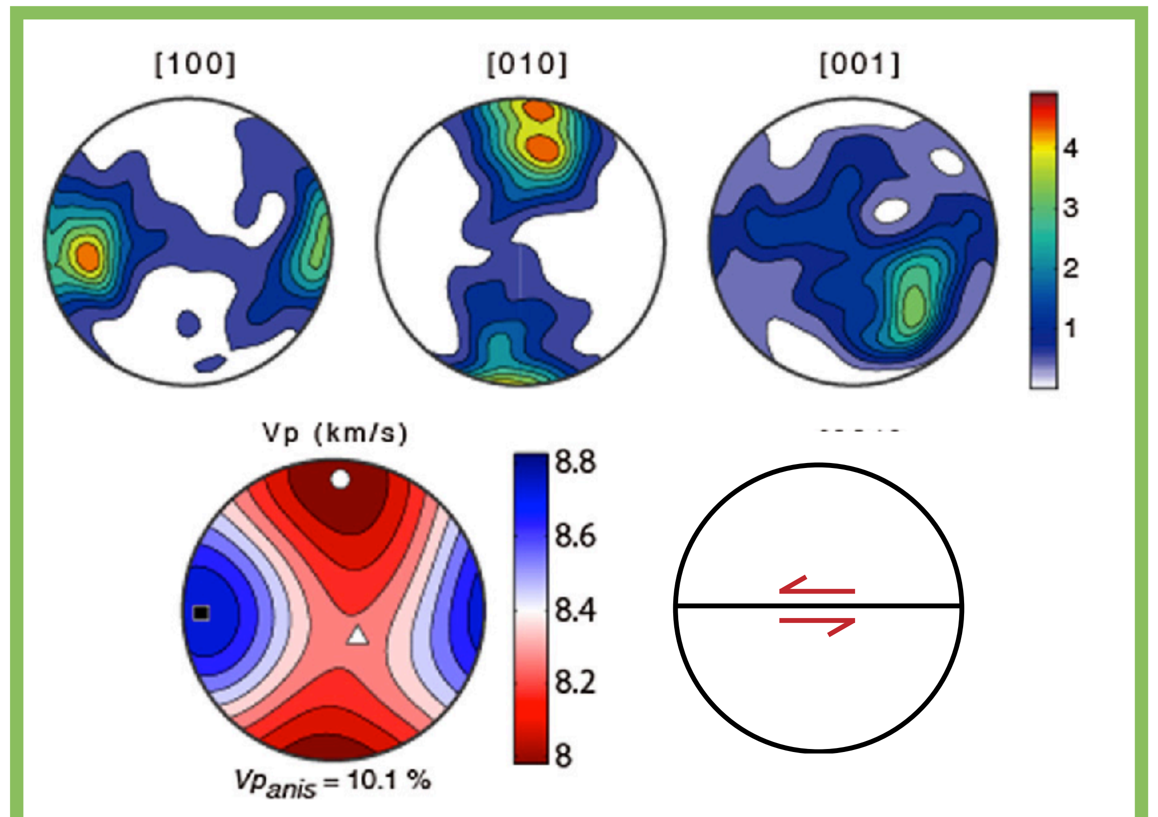

Michibayashi et al., 2016 EPSL

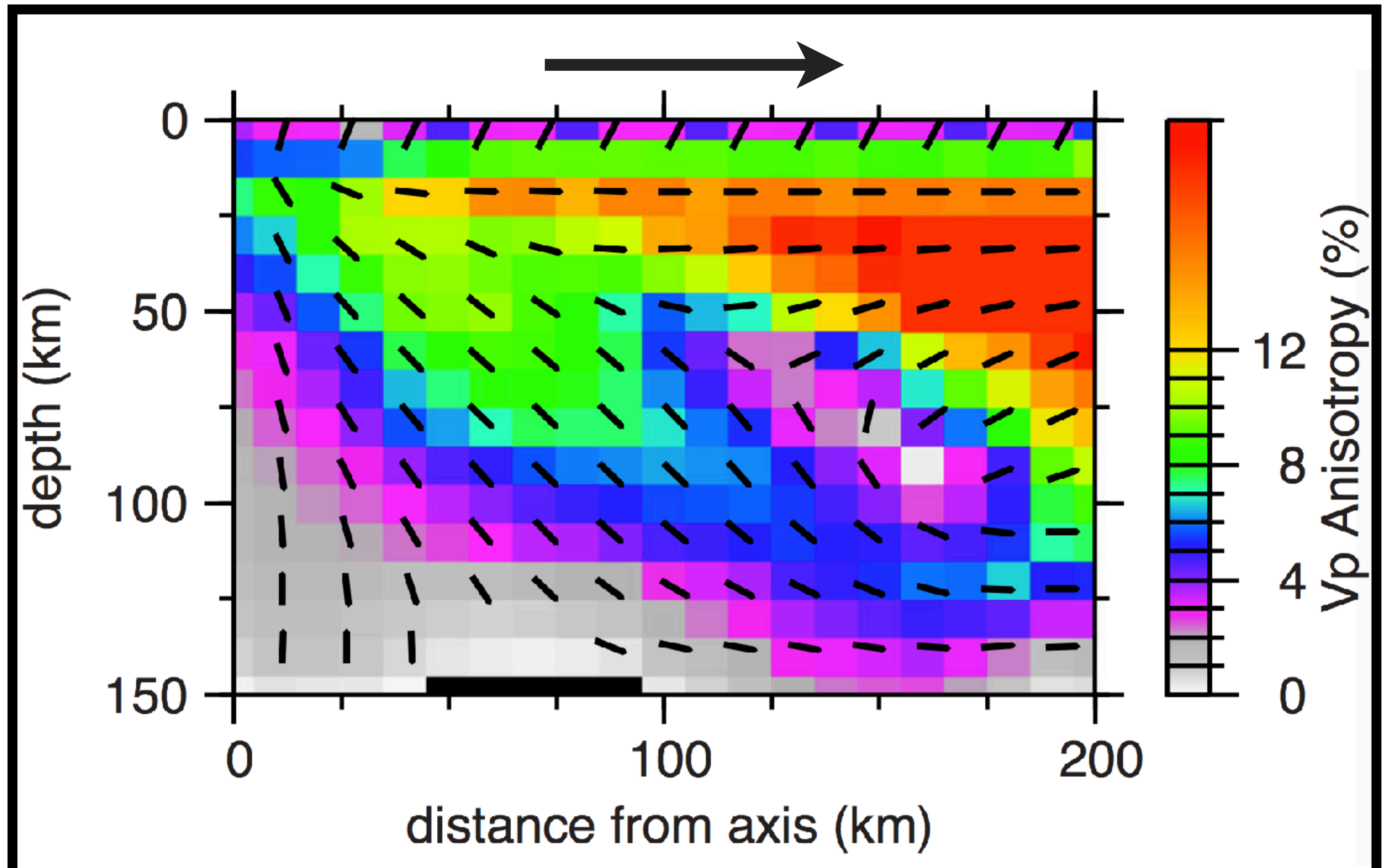

Blackman et al., 2017 GJI

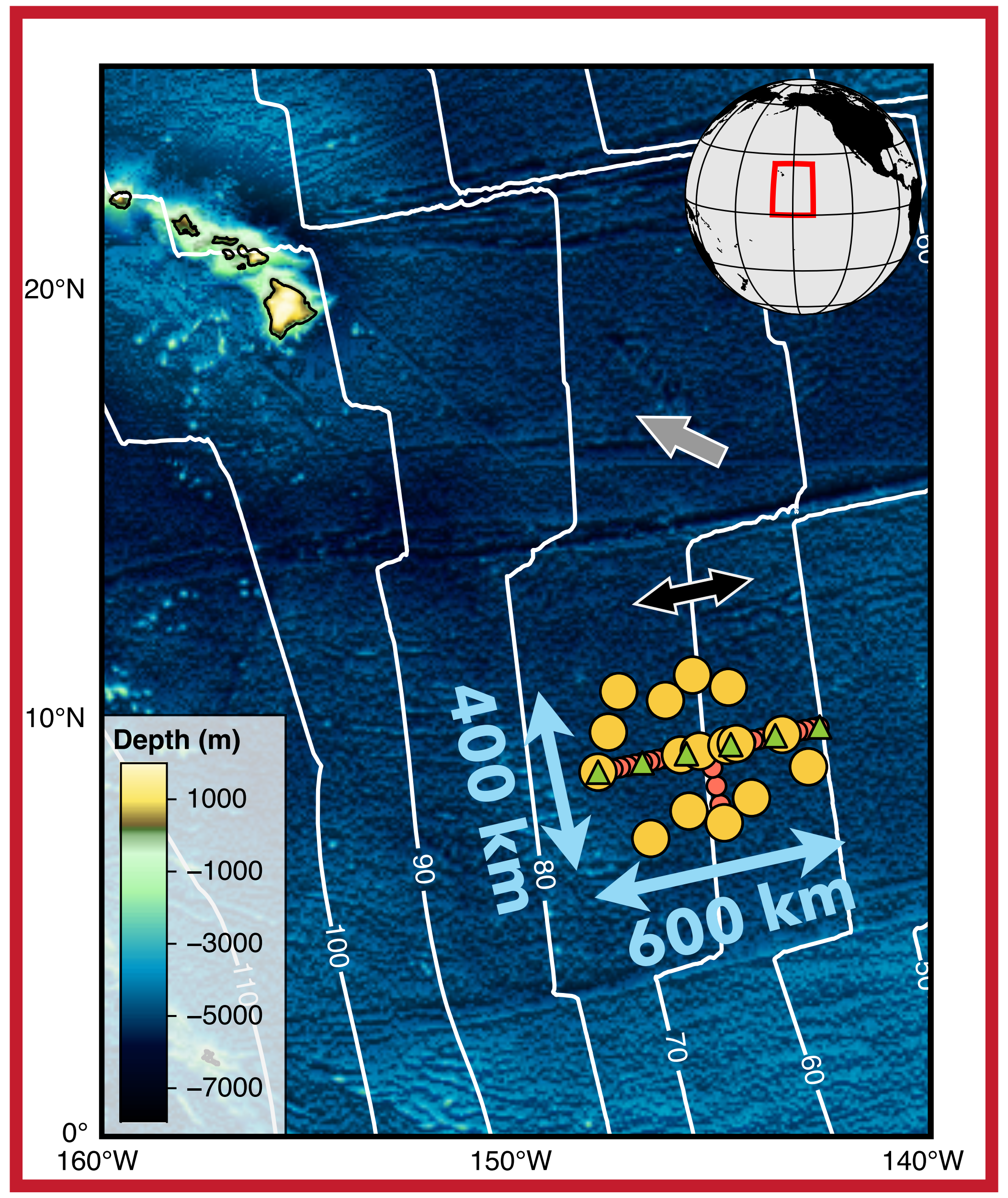

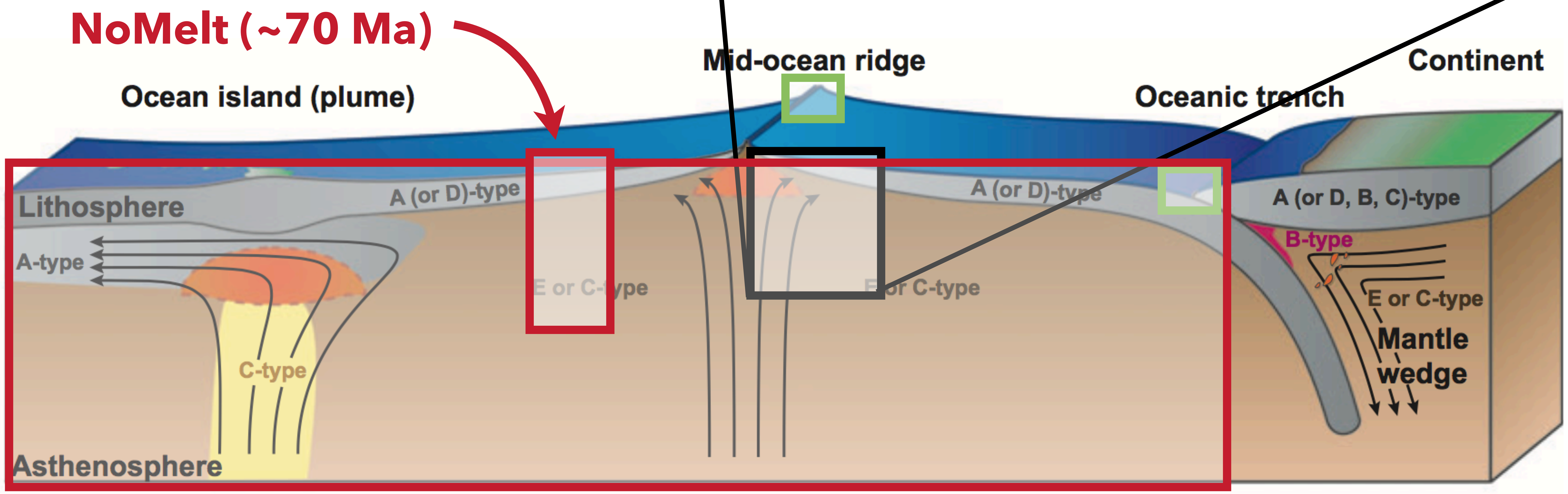

Karato et al., 2008 Annu. Rev.

Olivine LPO fabric types

LPO fabric development depends on **stress**, **H_2O content**, and **temperature**

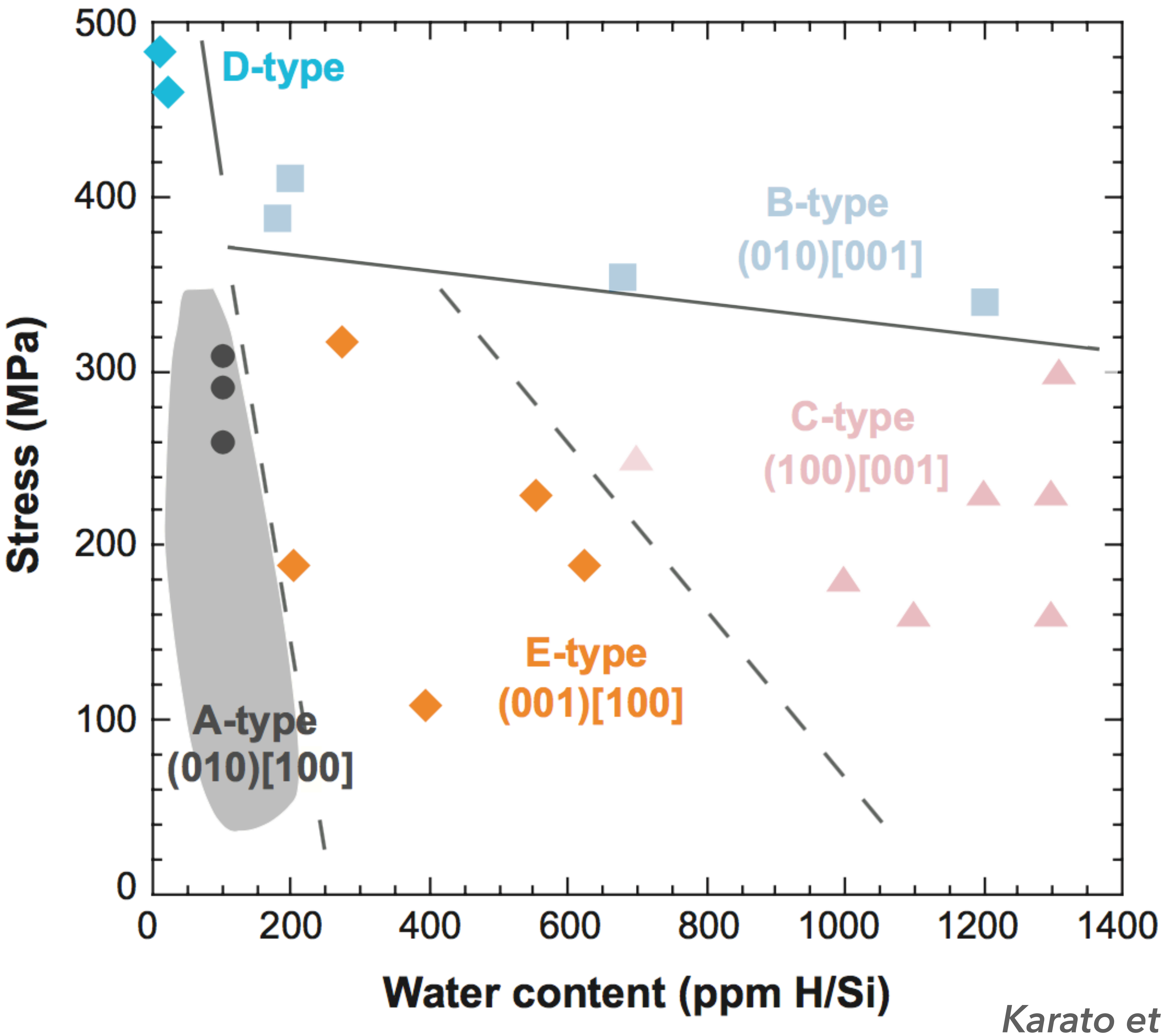

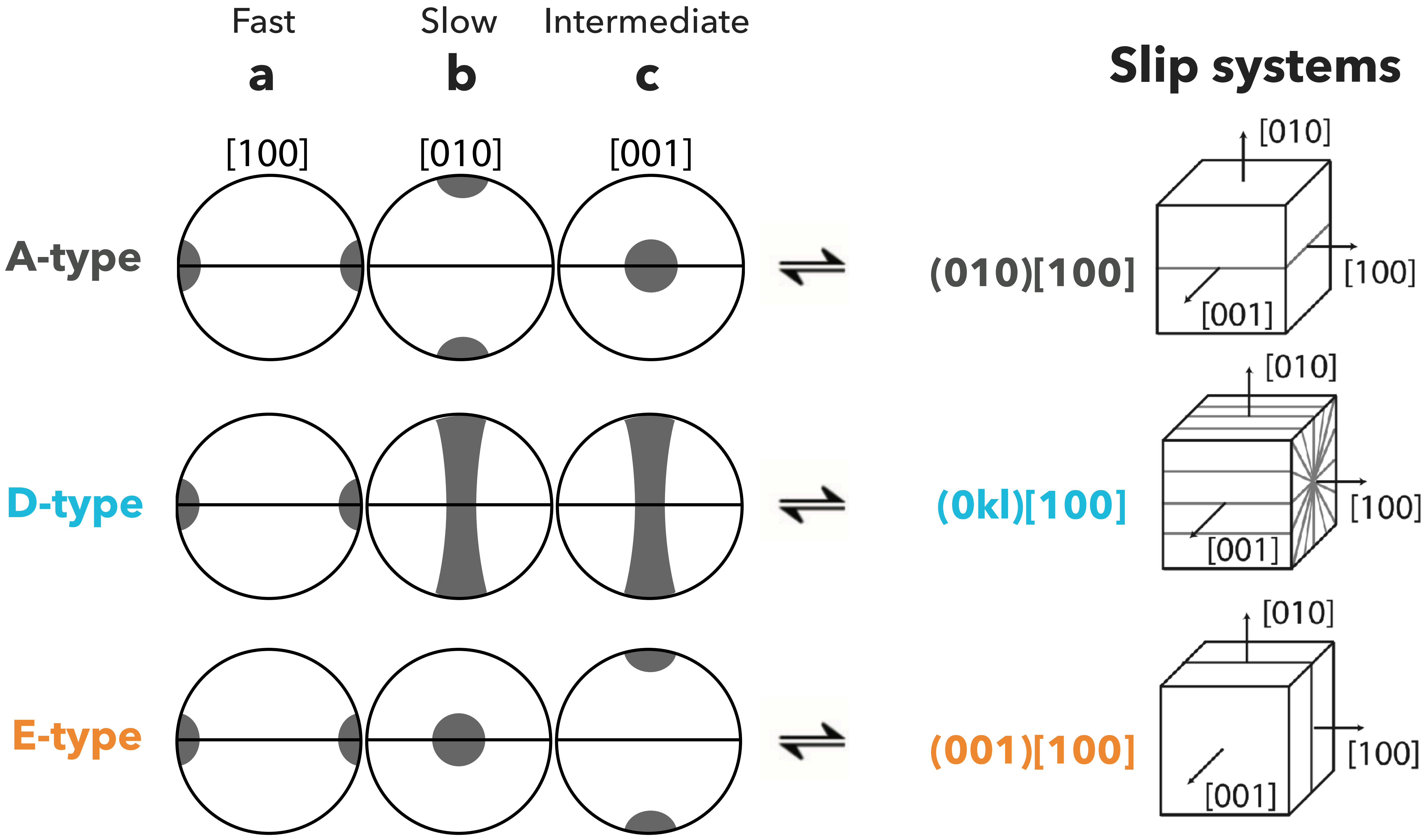

After Skemer et al., 2012 G3

Karato et al., 2008 Annu. Rev. ; Jung et al., 2006

NoMelt anisotropy observations

Surface Waves: Love 2θ & 4θ (5–7.5 s) Rayleigh 2θ (5–150 s)

Love
7.5 s

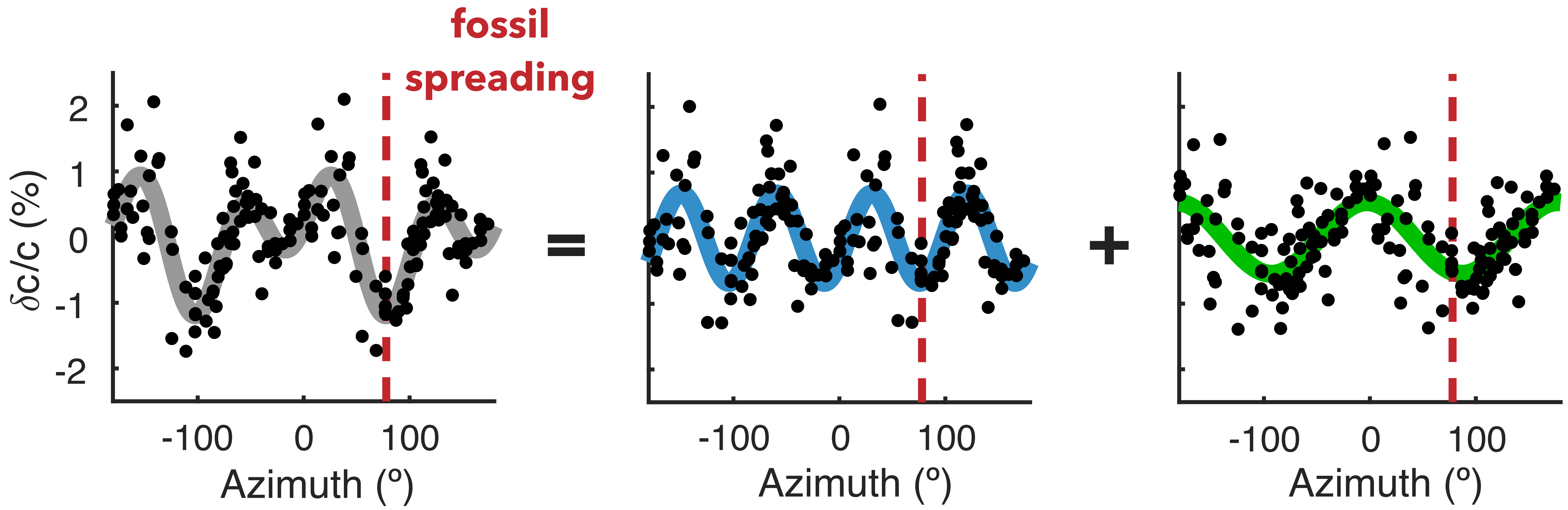

Russell et al. in review

NoMelt anisotropy observations

Surface Waves:

Love 2θ & 4θ (5–7.5 s)
Rayleigh 2θ (5–150 s)

Love 7.5 s

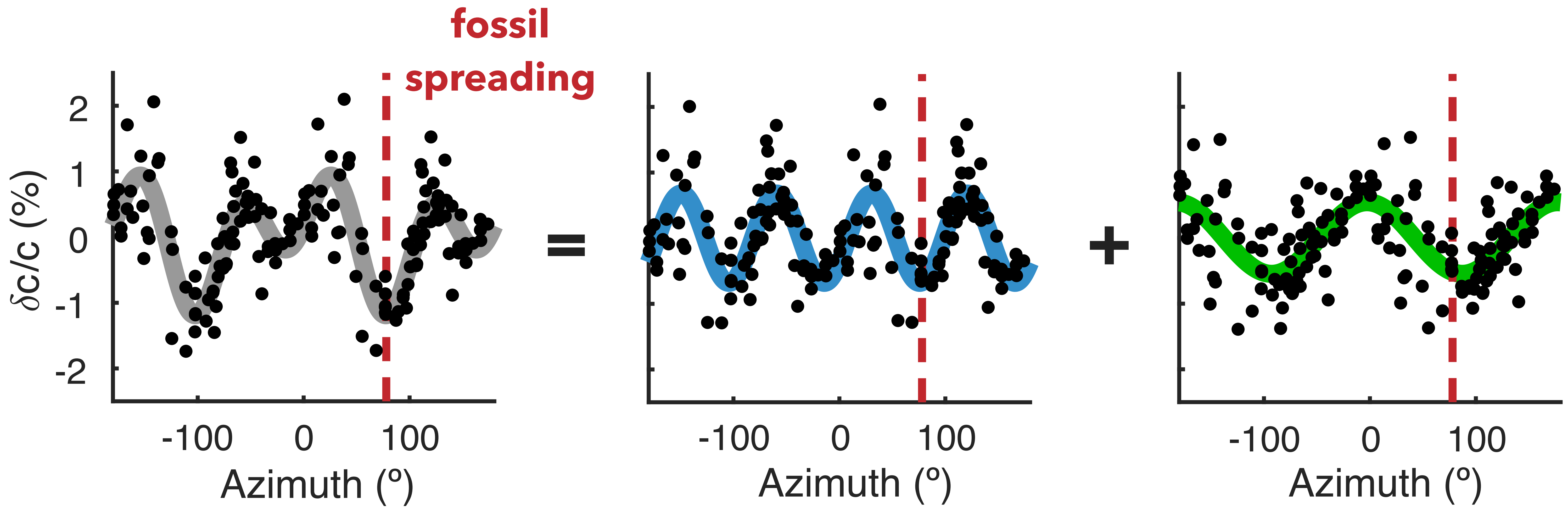

Rayleigh 7.5 s

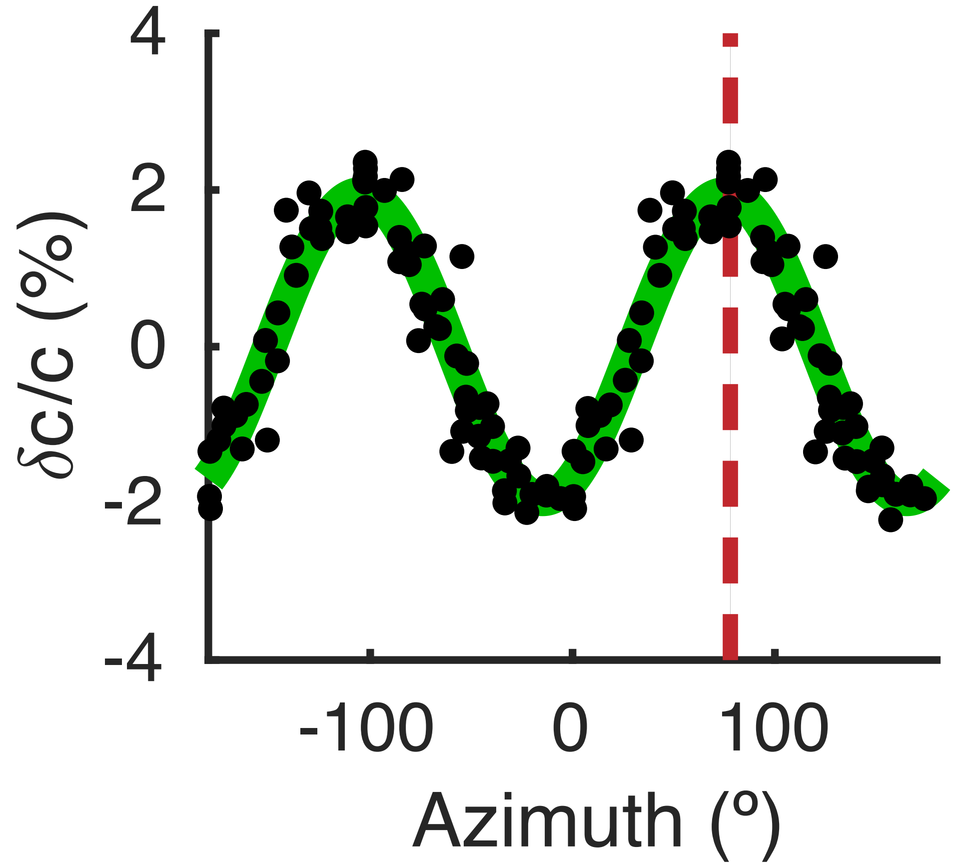

Shear Parameters
G: 2θ variation of V_{SV}
E: 4θ variation of V_{SH}

Russell et al. in review

NoMelt anisotropy observations

Surface Waves:
Love 2θ & 4θ (5-7.5 s)
Rayleigh 2θ (5-150 s)

Love 7.5 s

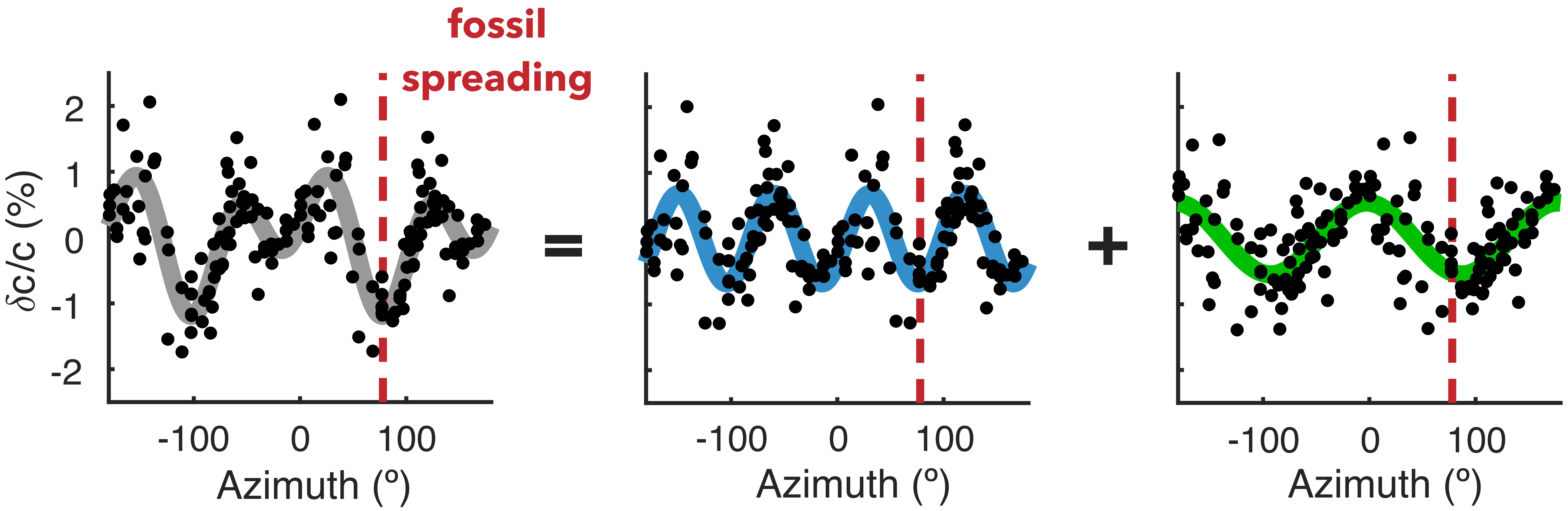

Rayleigh 7.5 s

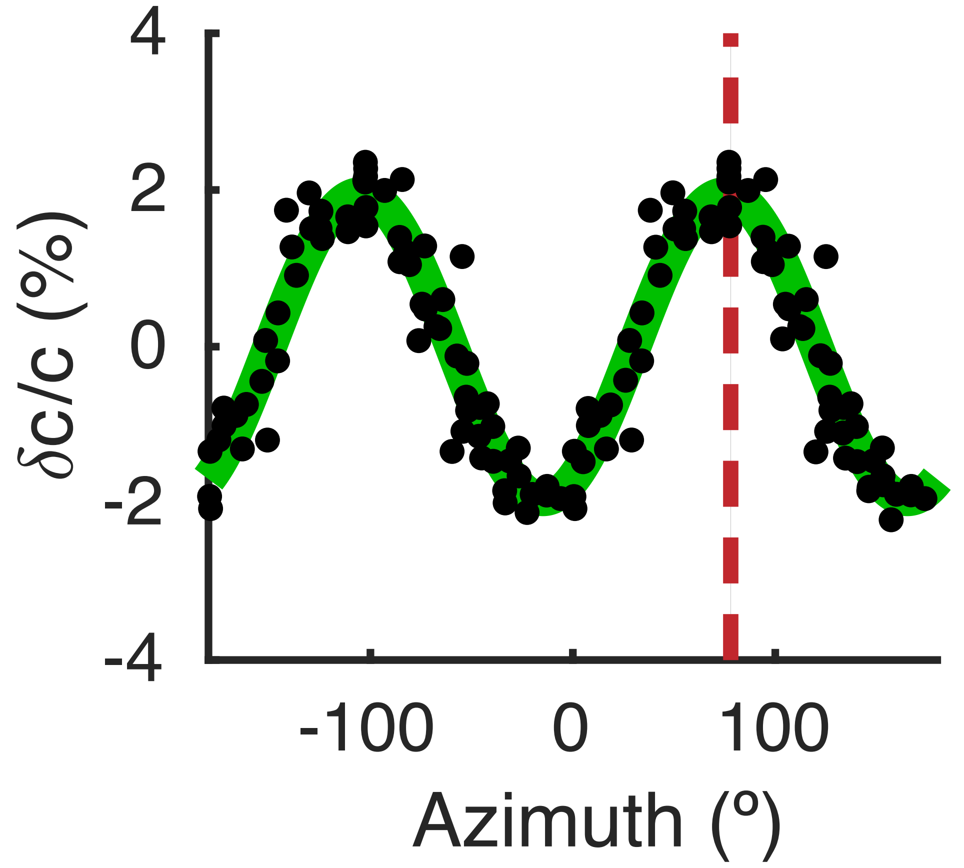

Shear Parameters
G: 2θ variation of V_{SV}
E: 4θ variation of V_{SH}

Pn anisotropy

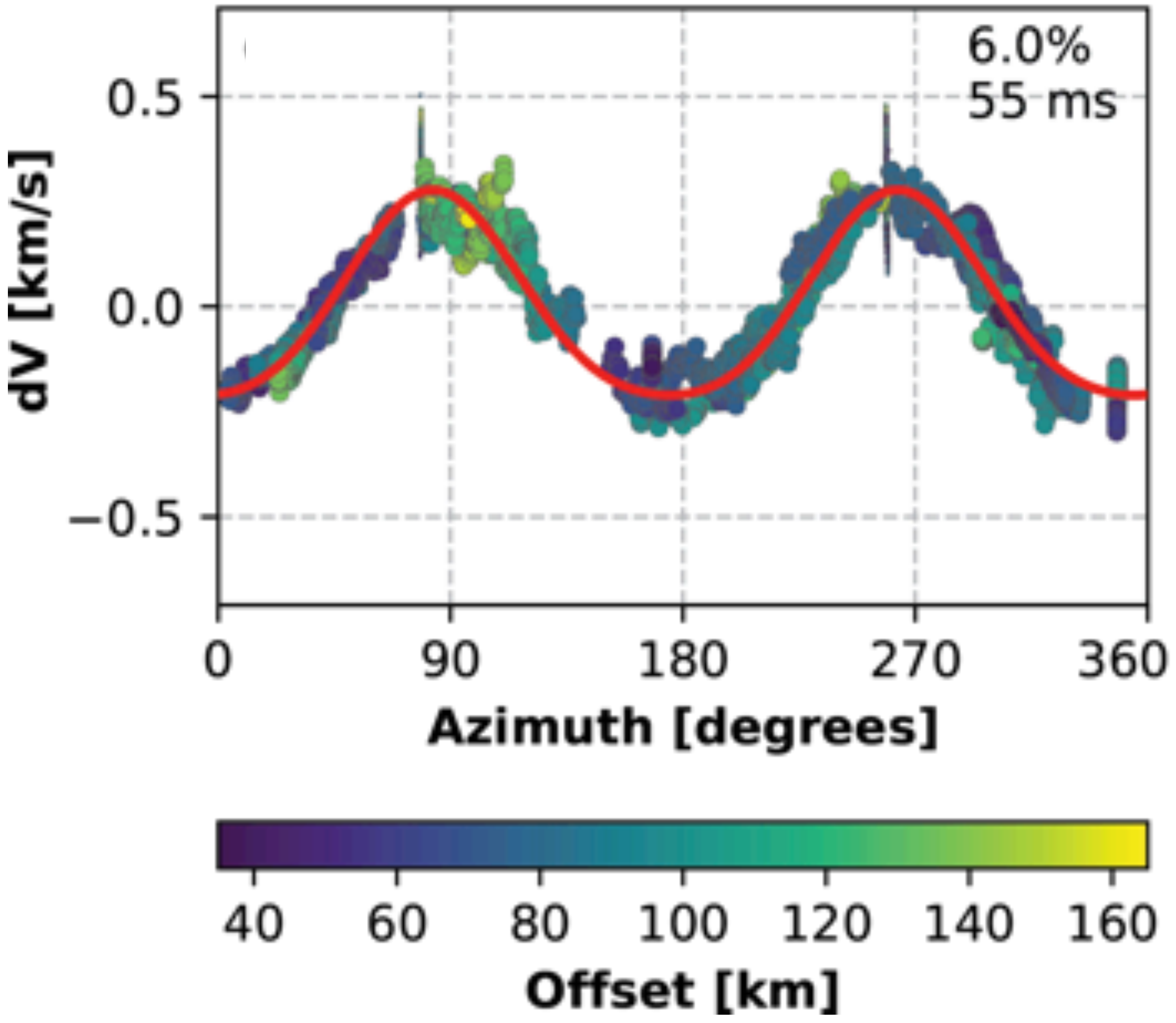

Compressional Parameters
B: 2θ variation of V_P

Russell et al. in review

Mark et al. in review

Constraining the elastic tensor (C_{ij})

13 elastic parameters required to constrain 13 elements of C_{ij}

$$C_{ij} = \begin{pmatrix} A + B_c + E_c & A - 2N - E_c & F + H_c & 0 & 0 & \frac{1}{2}B_s + E_s \\ \cdot & A - B_c + E_c & F - H_c & 0 & 0 & \frac{1}{2}B_s - E_s \\ \cdot & \cdot & C & 0 & 0 & H_s \\ \cdot & \cdot & \cdot & L - G_c & G_s & 0 \\ \cdot & \cdot & \cdot & \cdot & L + G_c & 0 \\ \cdot & \cdot & \cdot & \cdot & \cdot & N - E_c \end{pmatrix}$$

Azimuthal Anisotropy:

$$\rho\, V_{qP}(\theta)^2 = A + B_c \cos(2\theta) + B_s \sin(2\theta) + E_c \cos(4\theta) + E_s \sin(4\theta)$$

$$\rho\, V_{qSV}(\theta)^2 = L + G_c \cos(2\theta) + G_s \sin(2\theta)$$

$$\rho\, V_{qSH}(\theta)^2 = N - E_c \cos(4\theta) - E_s \sin(4\theta)$$

Constraining the elastic tensor (C_{ij})

13 elastic parameters required to constrain 13 elements of C_{ij}

$$C_{ij} = \begin{pmatrix} A+B_c+E_c & A-2N-E_c & F+H_c & 0 & 0 & \frac{1}{2}B_s+E_s \\ \cdot & A-B_c+E_c & F-H_c & 0 & 0 & \frac{1}{2}B_s-E_s \\ \cdot & \cdot & C & 0 & 0 & H_s \\ \cdot & \cdot & \cdot & L-G_c & G_s & 0 \\ \cdot & \cdot & \cdot & \cdot & L+G_c & 0 \\ \cdot & \cdot & \cdot & \cdot & \cdot & N-E_c \end{pmatrix}$$

Rayleigh waves (2θ)
- **L**, **G**, B, H (V_{SV})

Love waves (2θ, 4θ)
- **N**, **E**, G (V_{SH})

Pn (2θ, 4θ)
- **A**, **B**, E (V_{PH})

}

9 terms

Scaling relations
- C, H, F (V_{PV})
- A, B below 7 km

}

4 terms

$C_{ij} =$

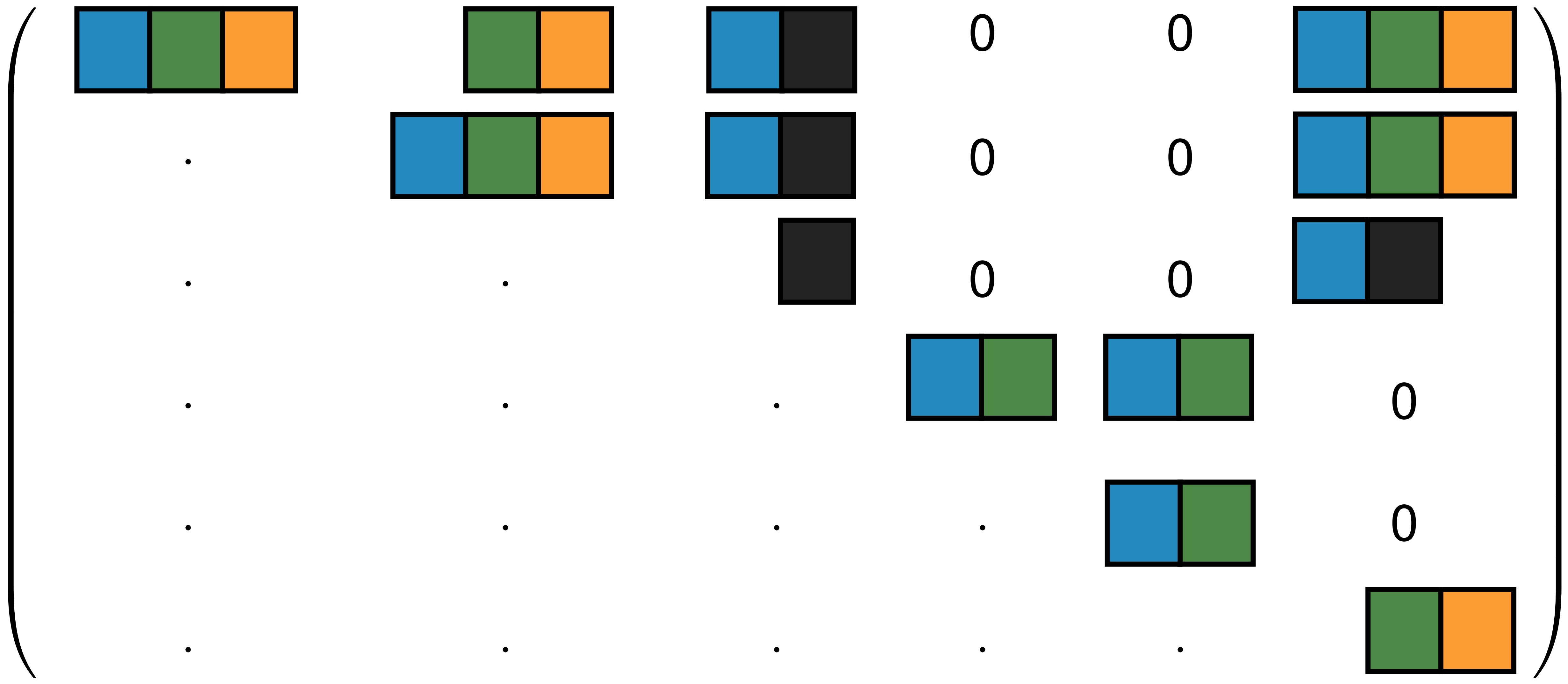

Elastic model

Vs, ξ, G, B, H, E,
Ψ_G, Ψ_B, Ψ_H, Ψ_E

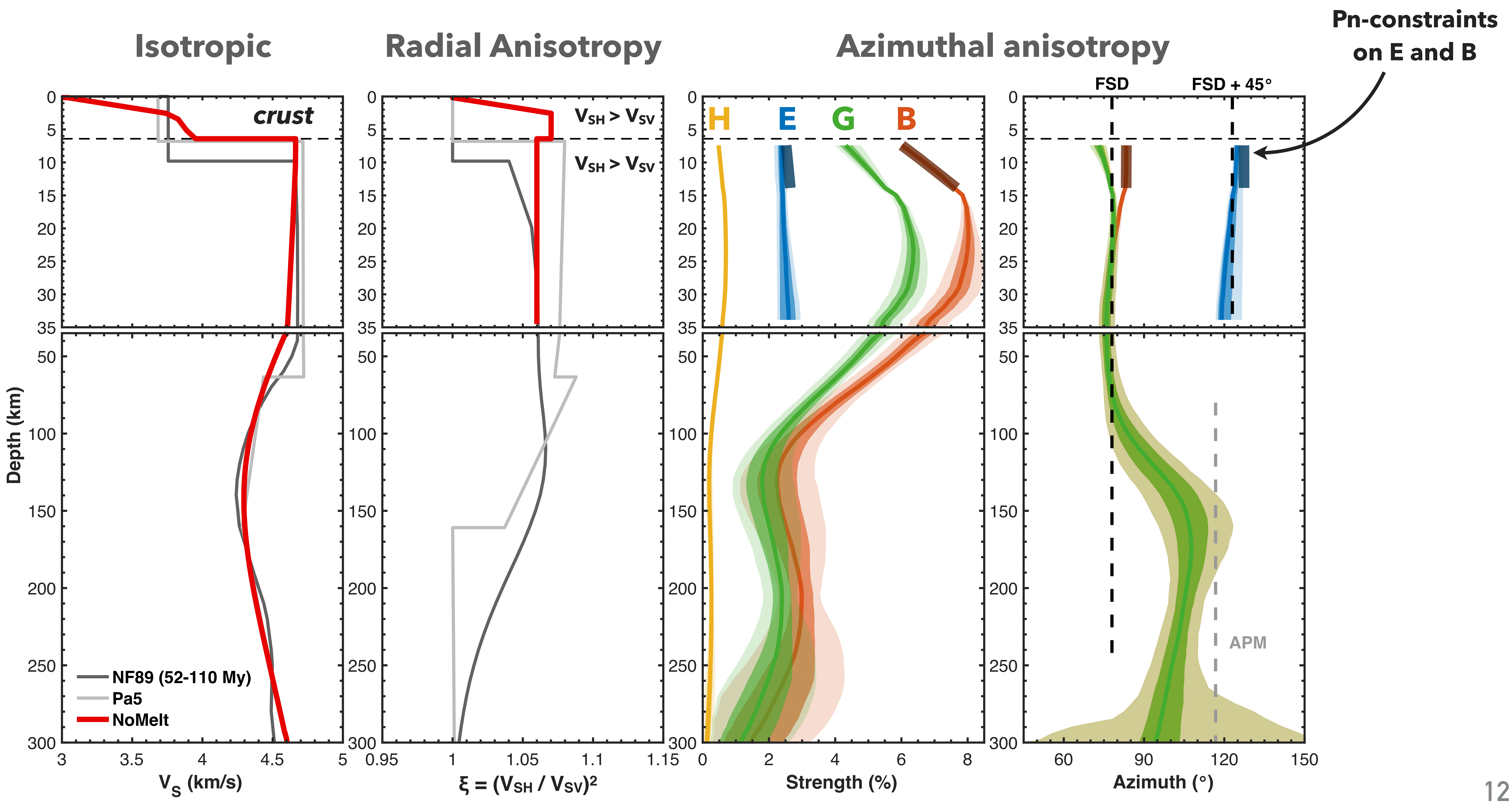

Elastic model

Vs, ξ, G, B, H, E,
Ψ_G, Ψ_B, Ψ_H, Ψ_E

Comparison to petrofabrics

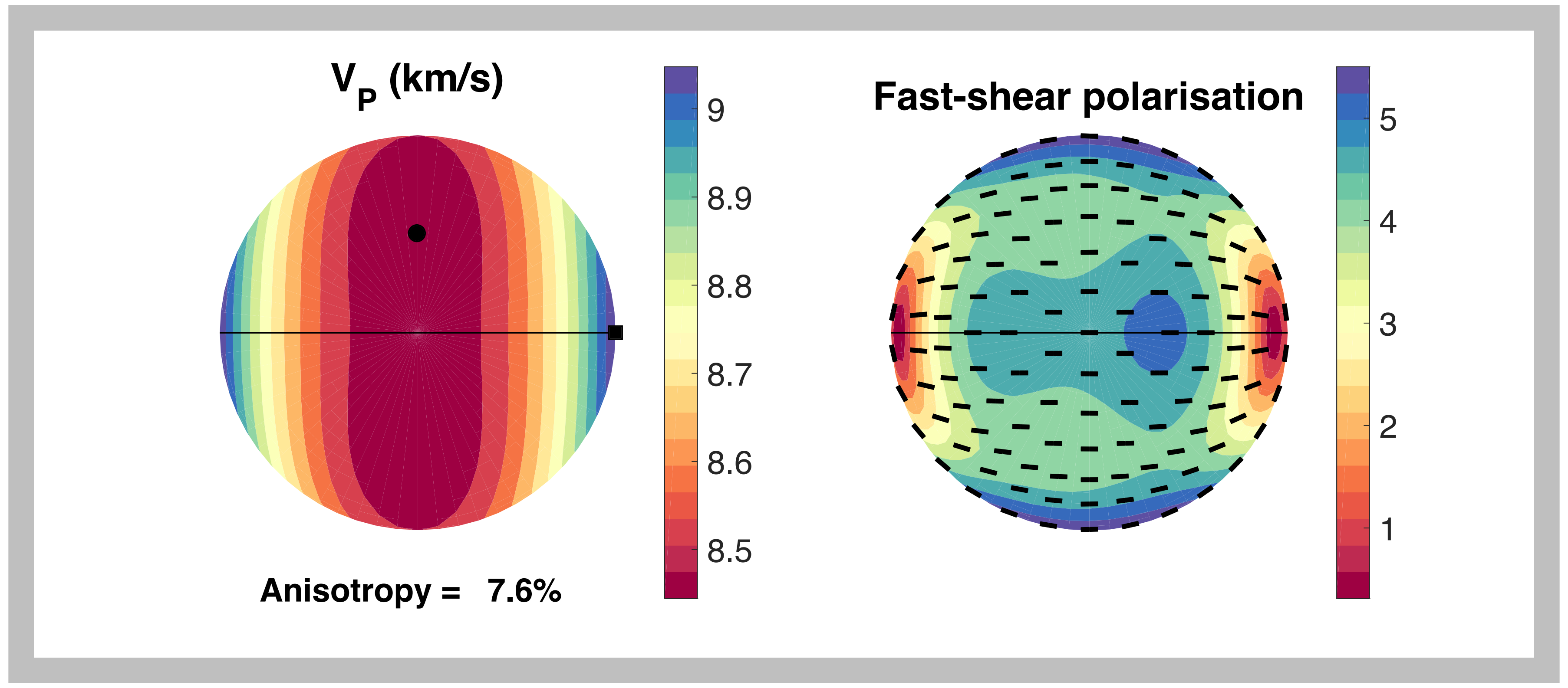

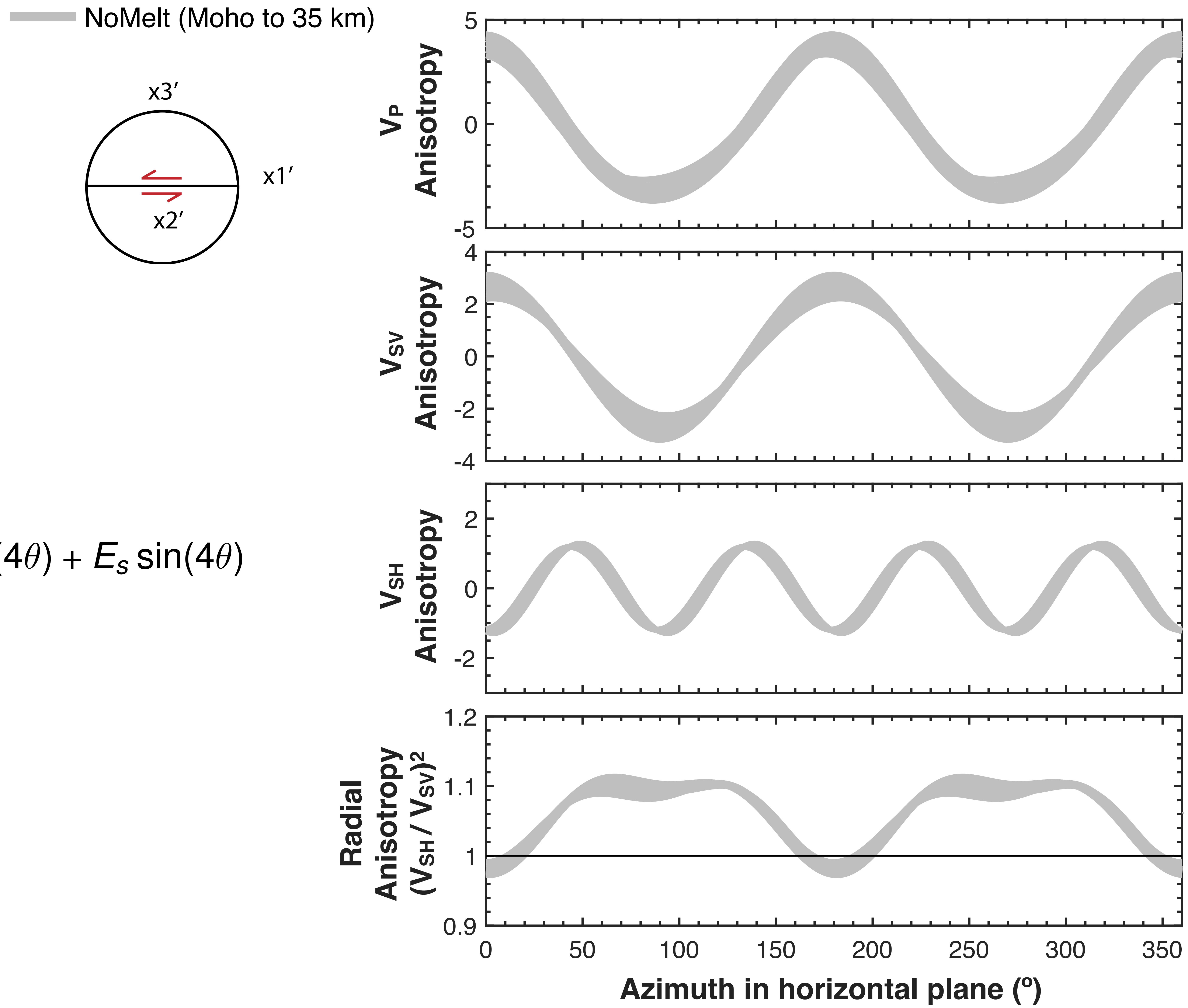

Azimuthal Anisotropy:

$$\rho\, V_{qP}(\theta)^2 \quad = \quad A + B_c \cos(2\theta) + B_s \sin(2\theta) + E_c \cos(4\theta) + E_s \sin(4\theta)$$

$$\rho\, V_{qSV}(\theta)^2 \quad = \quad L + G_c \cos(2\theta) + G_s \sin(2\theta)$$

$$\rho\, V_{qSH}(\theta)^2 \quad = \quad N - E_c \cos(4\theta) - E_s \sin(4\theta)$$

Comparison to petrofabrics

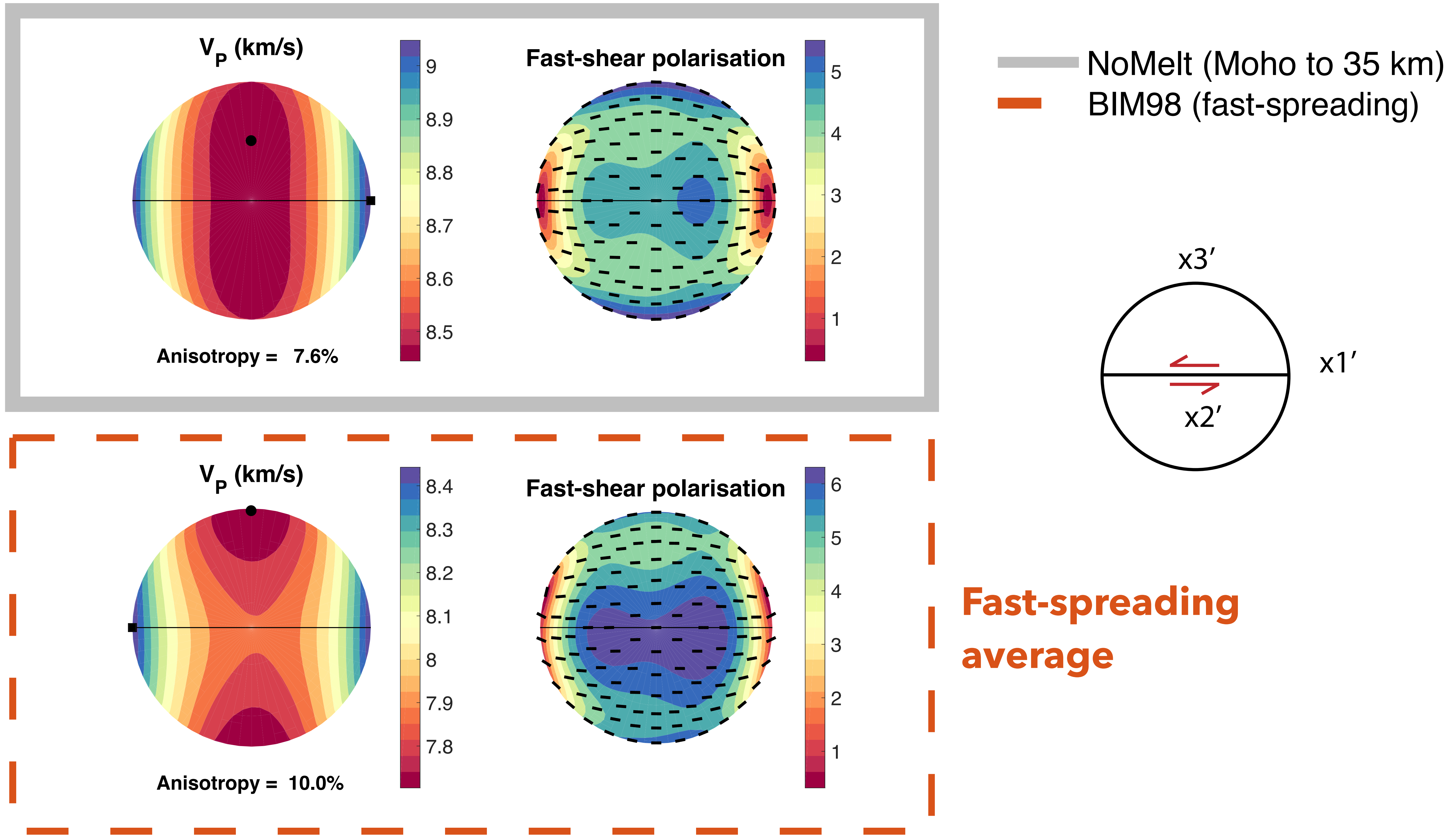

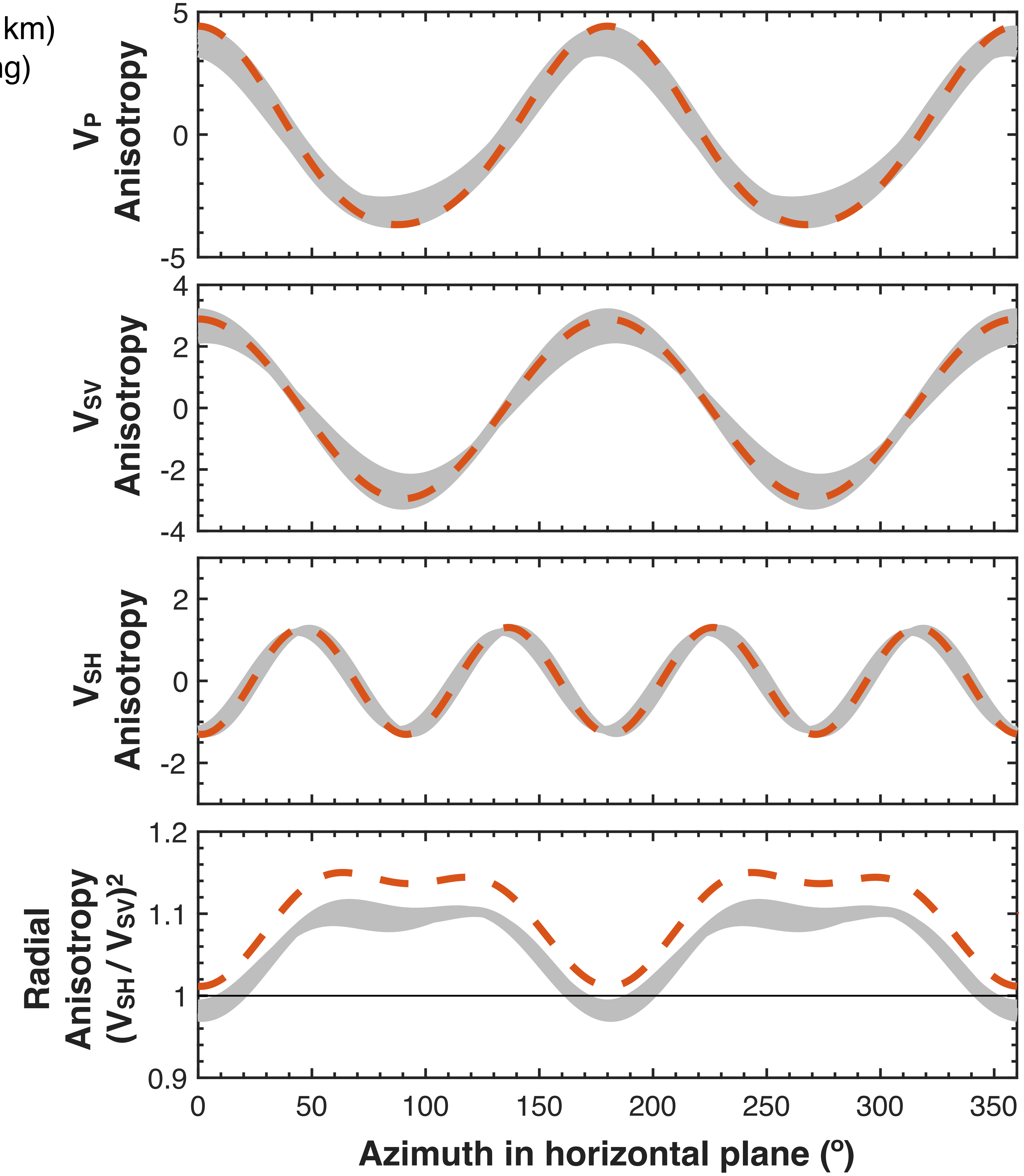

- Excellent agreement of azimuthal anisotropy
- NoMelt radial anisotropy is relatively weak

Comparison to petrofabrics

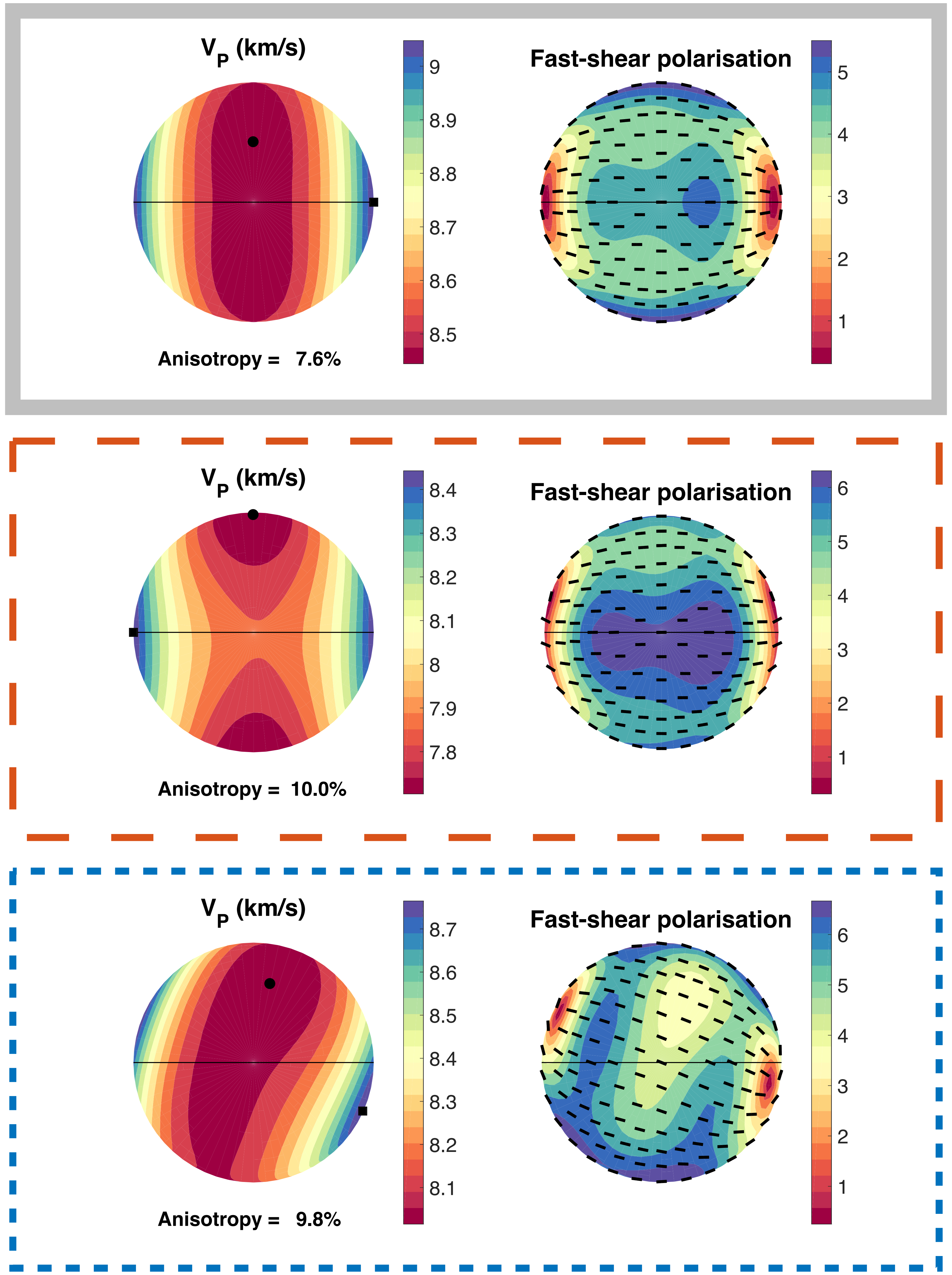

Fast-spreading average

Antalya ophiolite harzburgite

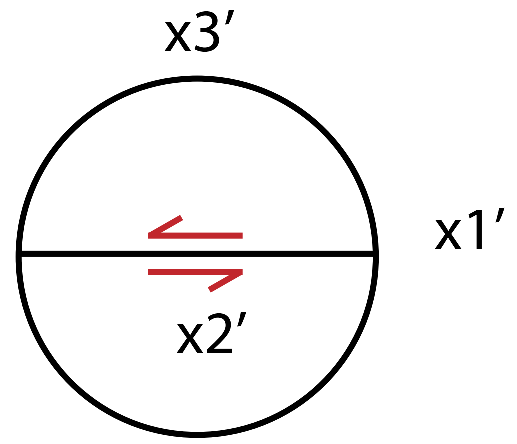

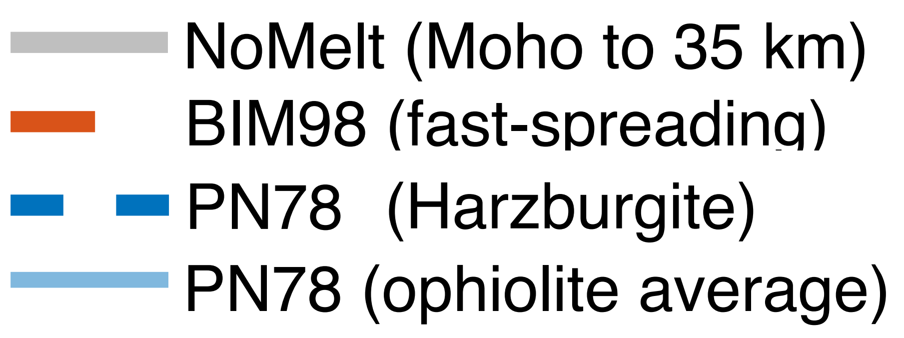

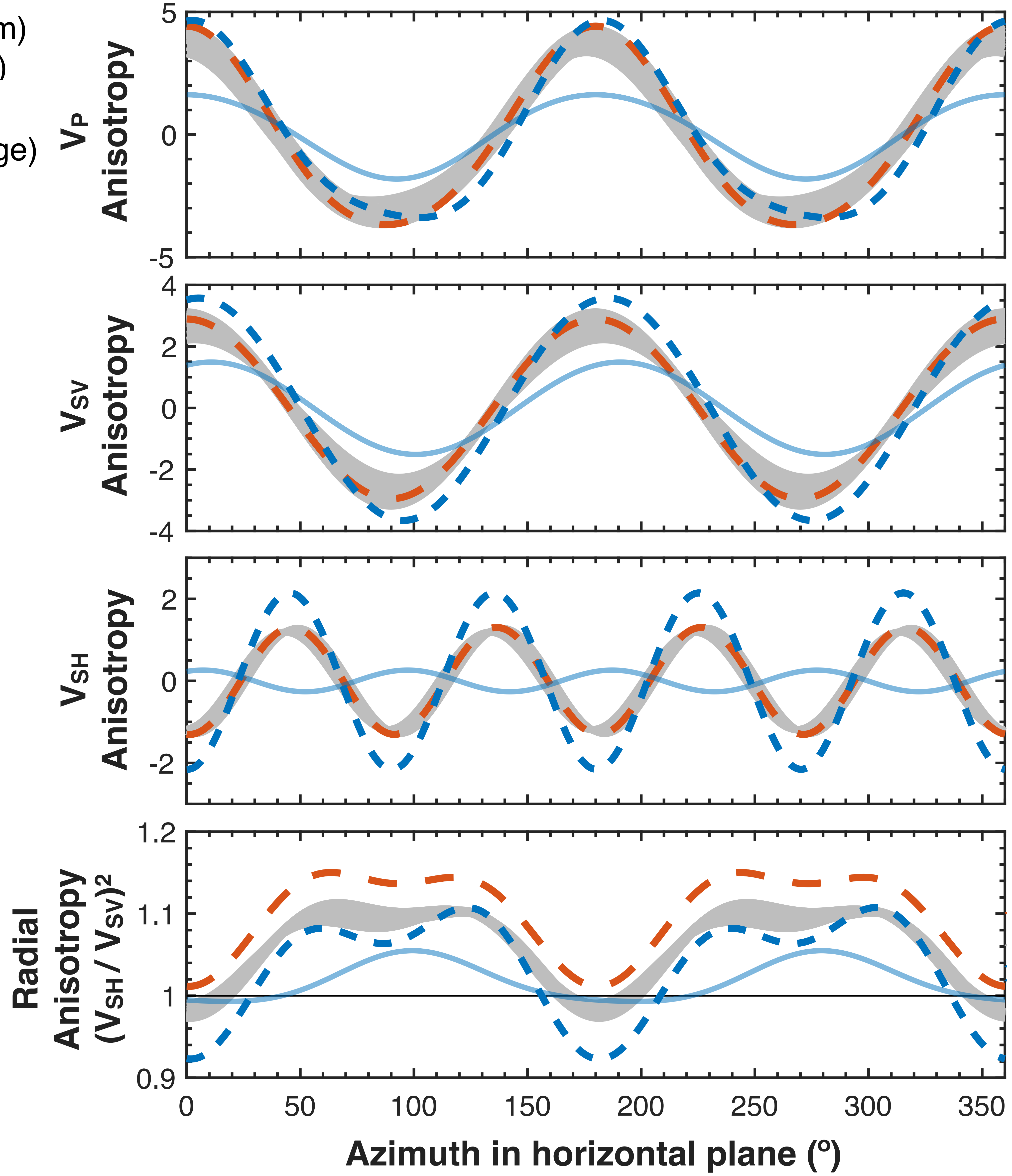

Comparison to petrofabrics: Rotated A-type fabric?

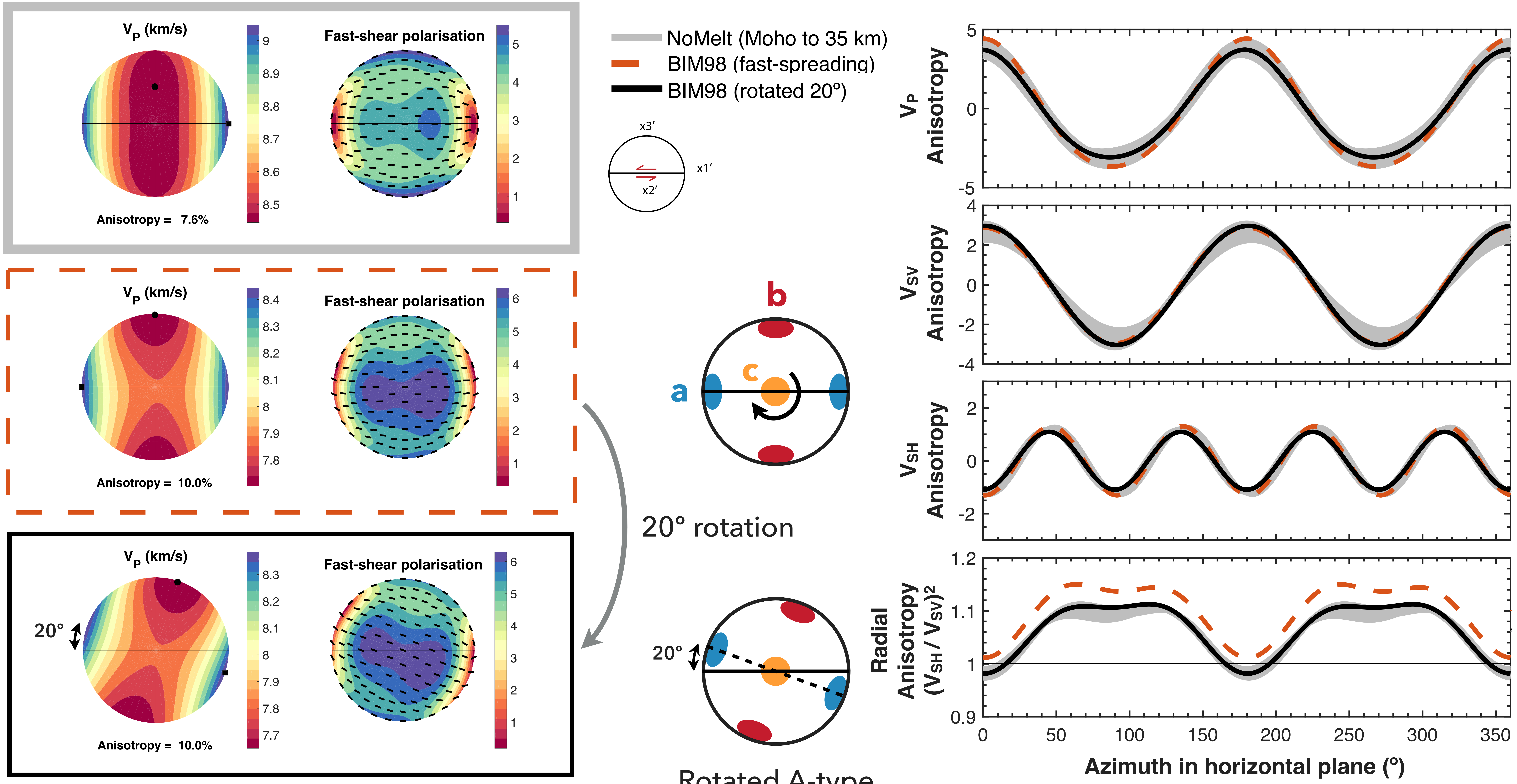

Rotated fabrics: observations

*a-axis rotation away from inferred shear plane ranging from **0°–60°** for natural and laboratory samples*

20°–25° is consistent with shear strain <200–300%

LPO evolution dependent on:

- finite strain
- pre-existing fabric
- deformation temperature
- orthopyroxene content
- grain size

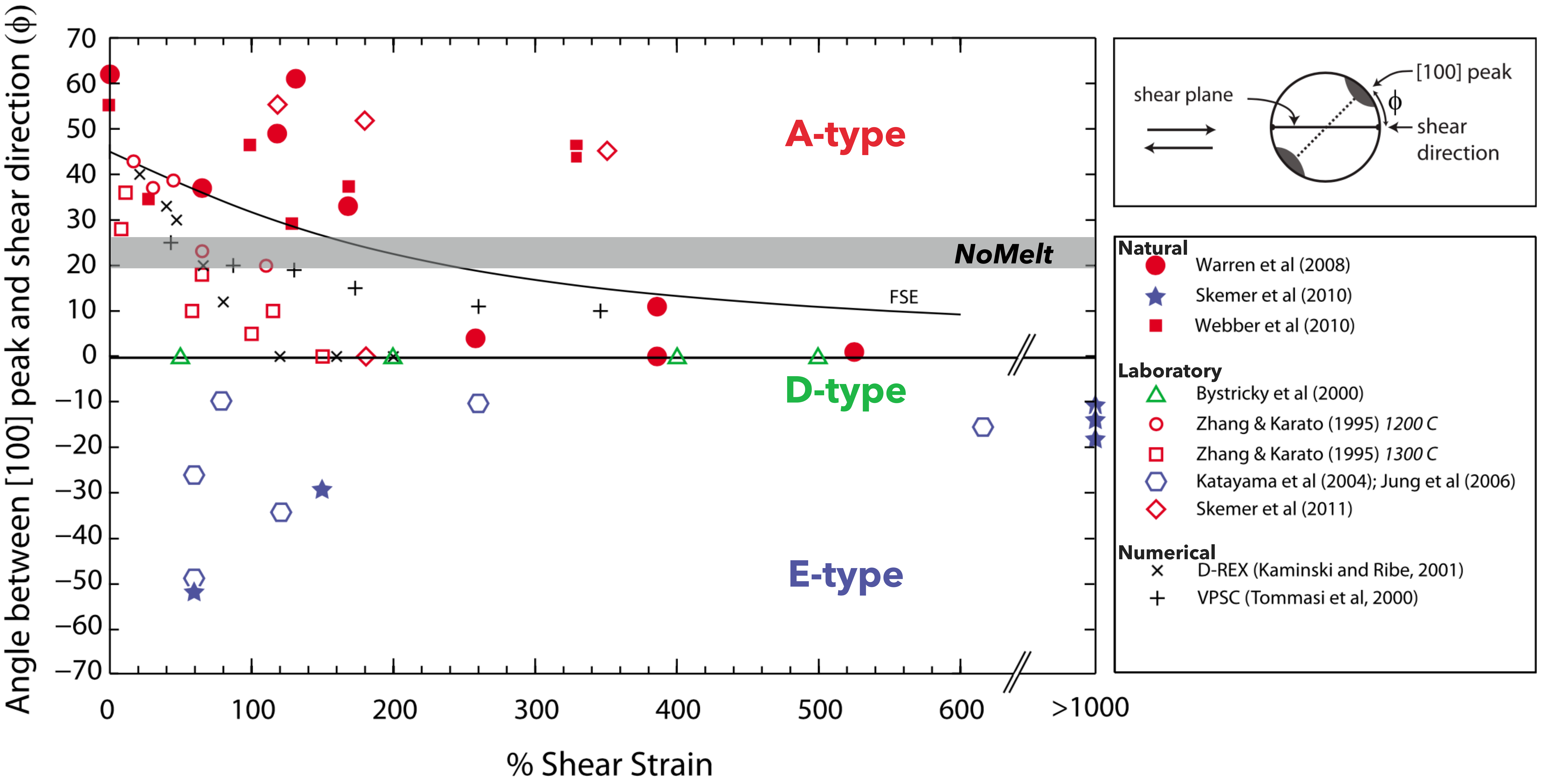

Skemer et al., 2012 G3

Rotated fabrics: geodynamic modeling

CPO development of fully-coupled, power-law (n=2), polycrystal material

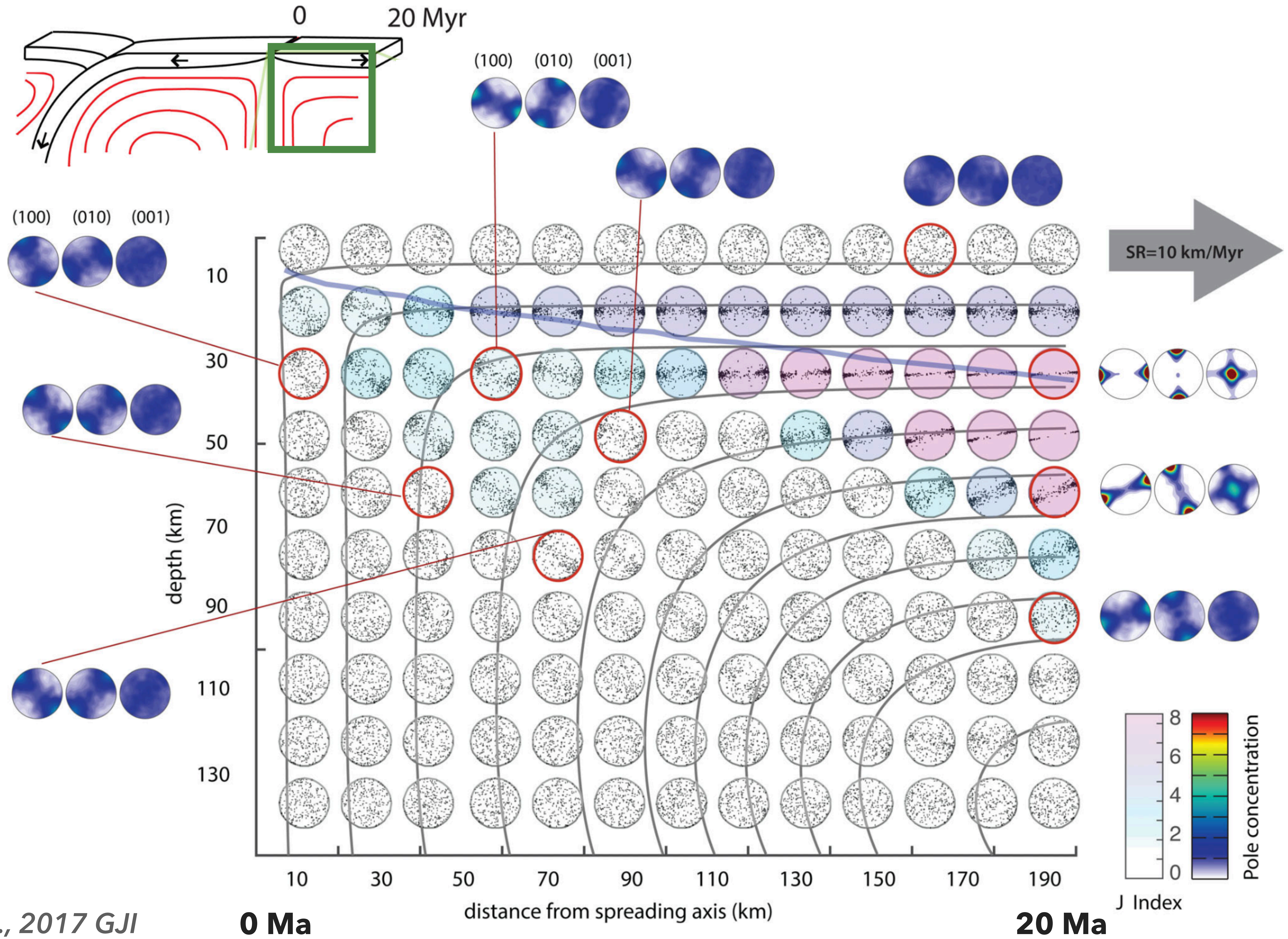

Blackman et al., 2017 GJI

0 Ma

20 Ma

Rotated fabrics: geodynamic modeling

CPO development of fully-coupled, power-law (n=2), polycrystal material

- lithospheric a-axes horizontally aligned
  - shear strains in the lithosphere too large
    - cooling rate?

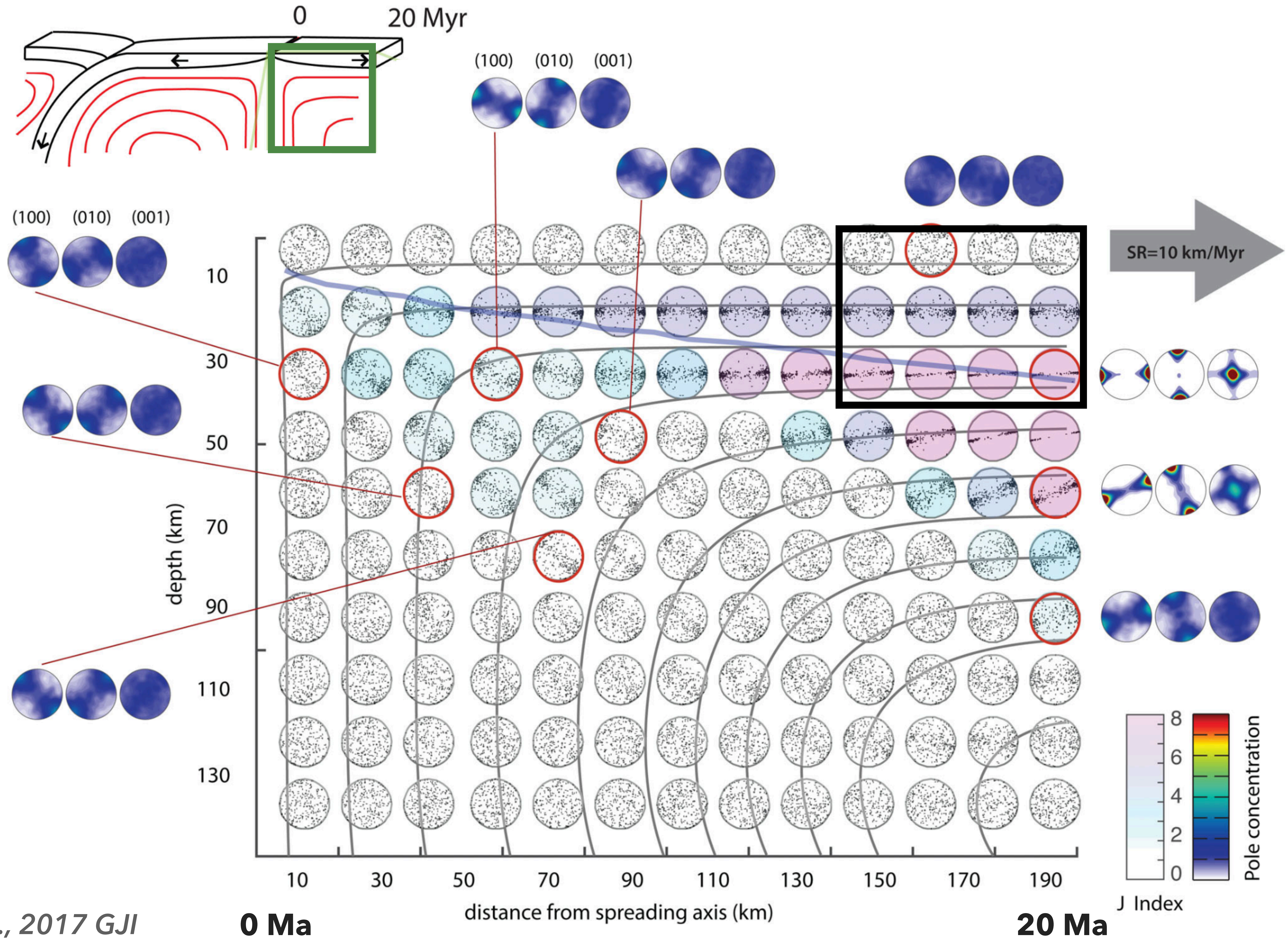

Blackman et al., 2017 GJI

0 Ma

20 Ma

Comparison to petrofabrics: E-type?

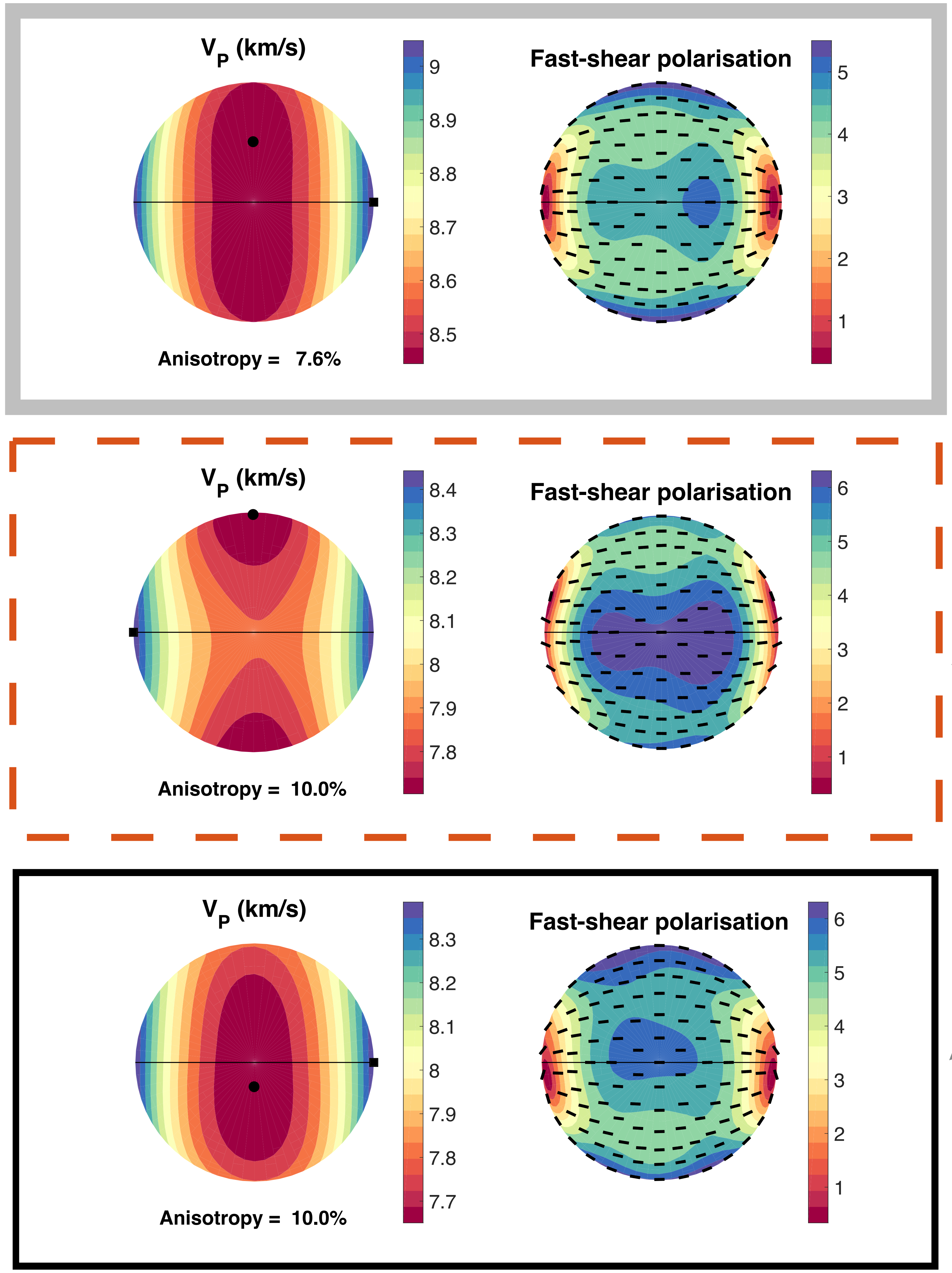

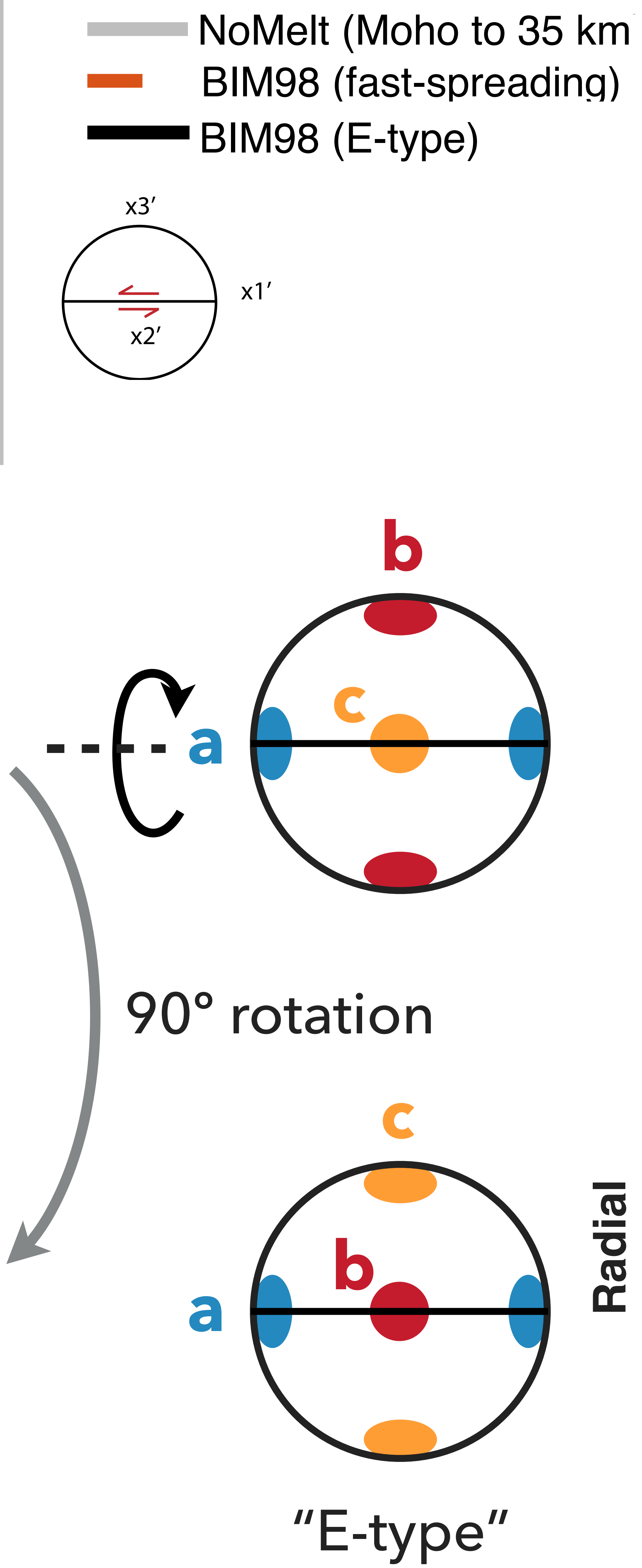

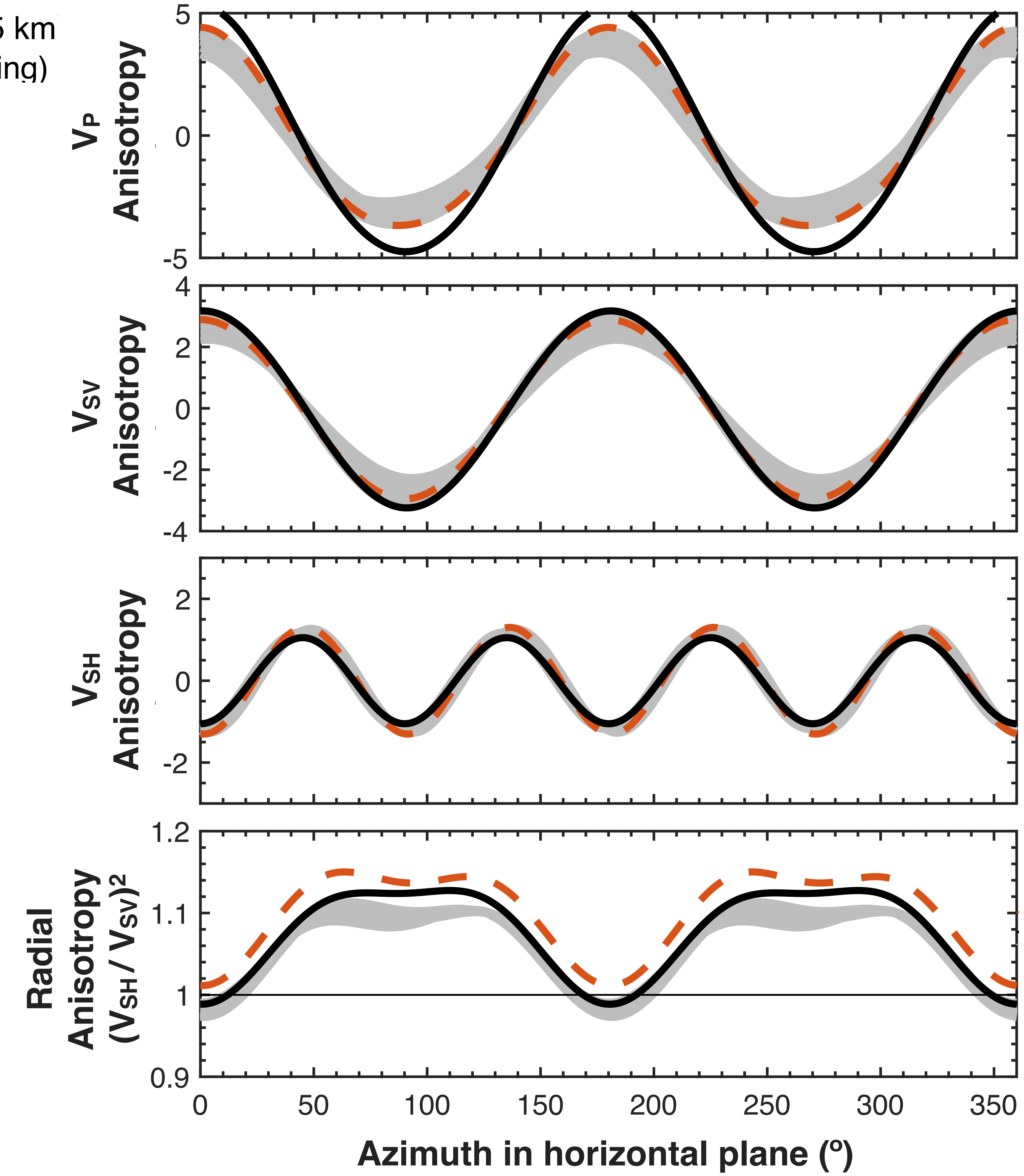

Comparison to petrofabrics: D-type?

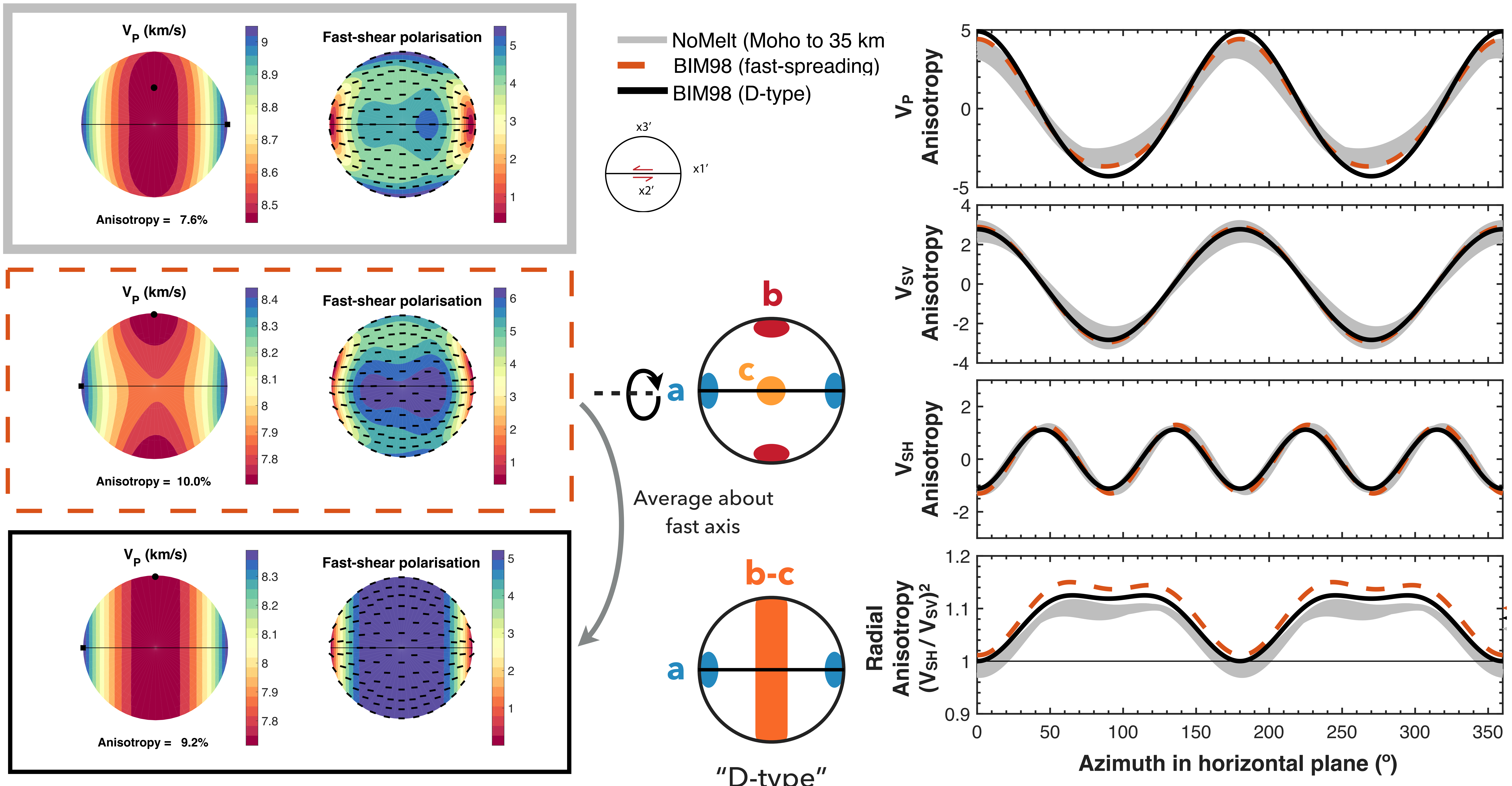

Fabric types

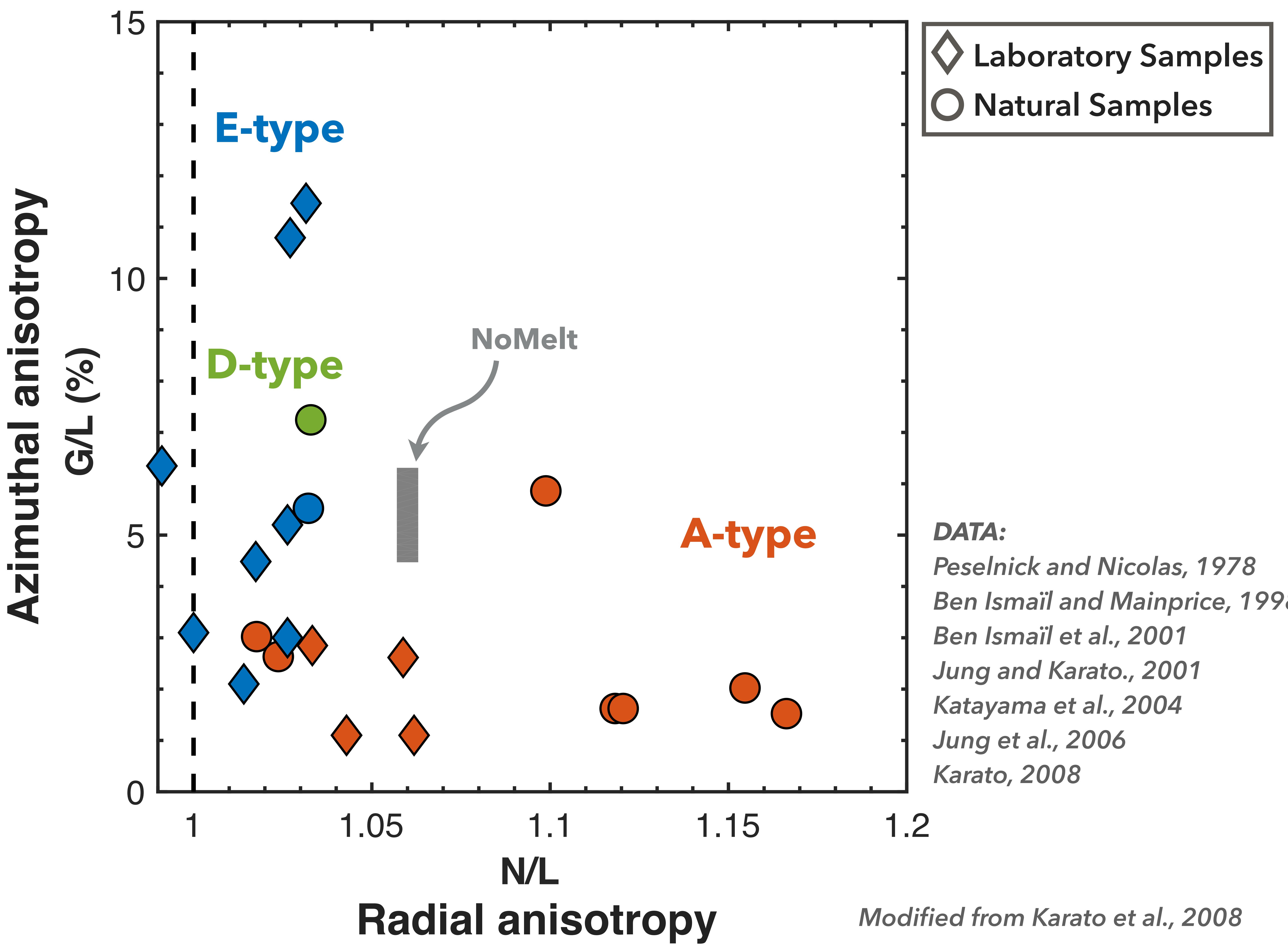

DATA:

Peselnick and Nicolas, 1978
Ben Ismaïl and Mainprice, 1998
Ben Ismaïl et al., 2001
Jung and Karato., 2001
Katayama et al., 2004
Jung et al., 2006
Karato, 2008

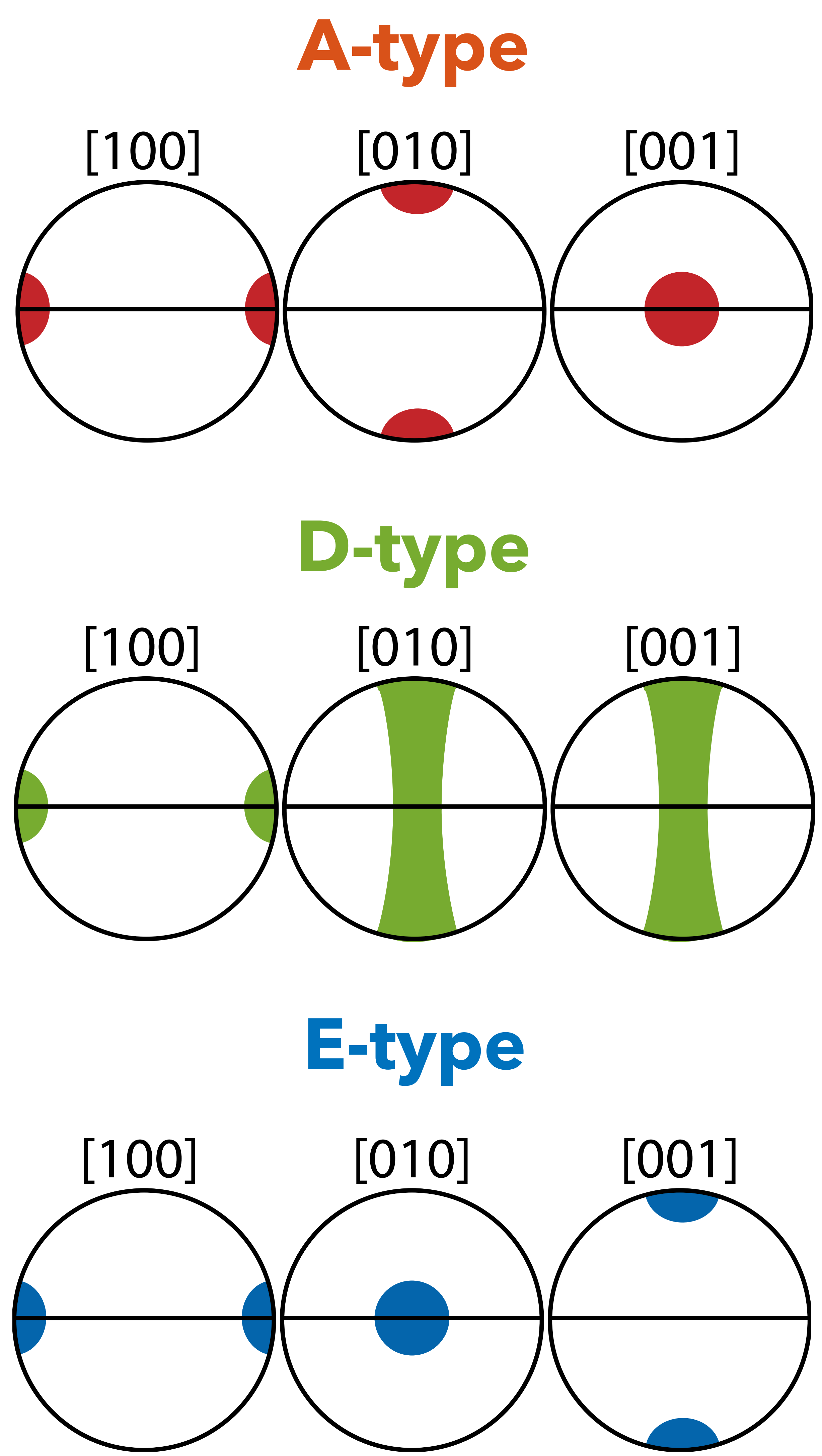

Modified from Karato et al., 2008

Conclusions

We model the full anisotropic variability of surface- and Pn-waves, providing a first in situ elastic tensor for 70 Ma oceanic lithosphere.

- Anisotropy **strength** and **direction** consistent with oceanic petrofabrics, bridging the gap between outcrop and seismic length scales
    - Remarkably coherent LPO alignment across NoMelt (~400x600km)
- **Strong** azimuthal anisotropy and relatively **weak** radial anisotropy consistent with:
    - (preferred) **A-type fabric rotated 20°-25°**, suggesting lithospheric shear strains < 200%-300%
    - or E-type fabric: moderate H_2O concentration during fabric formation near the ridge
    - or D-type fabric: high stress, low H_2O environment near ridge

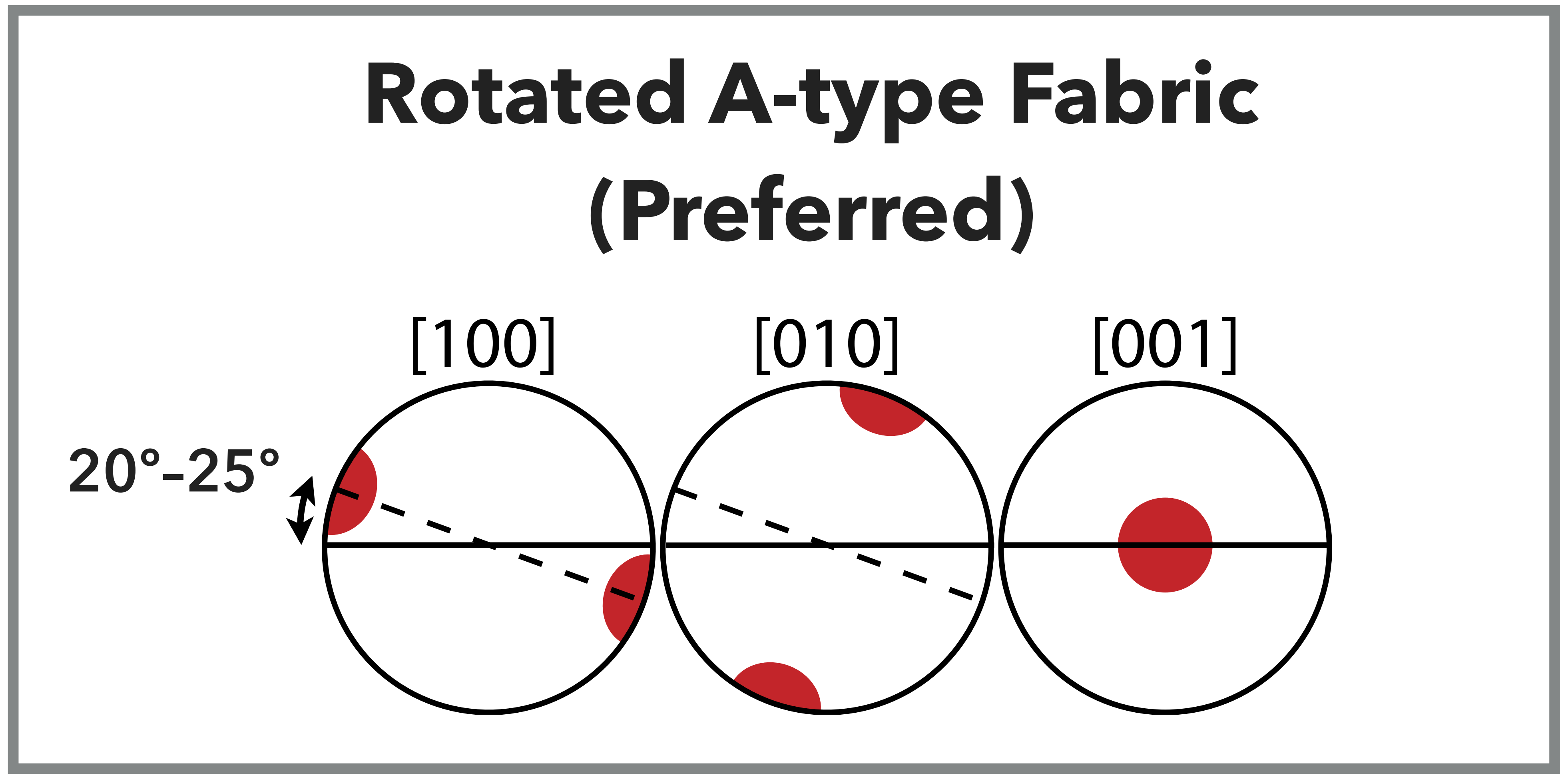

OR